

Error Probability and Capacity Analysis of Generalised Pre-Coding Aided Spatial Modulation

Rong Zhang, *Member, IEEE*, Lie-Liang Yang, *Senior Member, IEEE*, and Lajos Hanzo

Abstract—The recently proposed multiple input multiple output (MIMO) transmission scheme termed as generalized pre-coding aided spatial modulation (GPSM) is analyzed, where the key idea is that a particular subset of receive antennas is activated and the specific activation pattern itself conveys useful implicit information. We provide the upper bound of both the symbol error ratio (SER) and bit error ratio (BER) expression of the GPSM scheme of a low-complexity decoupled detector. Furthermore, the corresponding discrete-input continuous-output memoryless channel (DCMC) capacity as well as the achievable rate is quantified. Our analytical SER and BER upper bound expressions are confirmed to be tight by our numerical results. We also show that our GPSM scheme constitutes a flexible MIMO arrangement and there is always a beneficial configuration for our GPSM scheme that offers the same bandwidth efficiency as that of its conventional MIMO counterpart at a lower signal to noise ratio (SNR) per bit.

Index Terms—Author, please supply index terms/keywords for your paper. To download the IEEE Taxonomy go to http://www.ieee.org/documents/taxonomy_v101.pdf.

I. INTRODUCTION

MULTIPLE INPUT MULTIPLE OUTPUT (MIMO) systems constitute one of the most promising recent technical advances in wireless communications, since they facilitate high-throughput transmissions in the context of various standards [1]. Hence, they attracted substantial research interests, leading to the Vertical-Bell Laboratories Layered Space-Time (V-BLAST) scheme [2] and to the classic Space Time Block Coding (STBC) arrangement [3]. The point-to-point single-user MIMO systems are capable of offering diverse transmission functionalities in terms of multiplexing-diversity and beam-forming gains. Similarly, Spatial Division Multiple Access (SDMA) employed in the uplink and multi-user MIMO techniques invoked in the downlink also constitute beneficial building blocks [4], [5]. The basic benefits of MIMOs have also been recently exploited in the context of the network MIMO

concept [6], [7], for constructing large-scale MIMOs [8], [9] and for conceiving beneficial arrangements for interference-limited MIMO scenarios [10].

Despite having a plethora of studies on classic MIMO systems, their practical constraints, such as their I/Q imbalance, their transmitter and receiver complexity as well as the cost of their multiple Radio Frequency (RF) Power Amplifier (PA) chains as well as their Digital-Analogue/Analogue-Digital (DA/AD) converters have received limited attention. To circumvent these problems, low complexity alternatives to conventional MIMO transmission schemes have also been proposed, such as the Antenna Selection (AS) [11], [12] and the Spatial Modulation (SM) [13], [14] philosophies. More specifically, SM and generalised SM [15] constitute novel MIMO techniques, which were conceived for providing a higher throughput than a single-antenna aided system, while maintaining both a lower complexity and a lower cost than the conventional MIMOs, since they may rely on a reduced number of RF up-conversion chains. To elaborate a little further, SM conveys extra information by mapping $\log_2(N_t)$ bits to the Transmit Antenna (TA) indices of the N_t TAs, in addition to the classic modulation schemes, as detailed in [13].

By contrast, the family of Pre-coding aided Spatial Modulation (PSM) schemes is capable of conveying extra information by appropriately selecting the Receive Antenna (RA) indices, as detailed in [16]. More explicitly, in PSM the indices of the RA represent additional information in the spatial domain. As a specific counterpart of the original SM, PSM benefits from both a low cost and a low complexity at the receiver side, therefore it may be considered to be eminently suitable for downlink transmissions [16]. The further improved concept of Generalised PSM (GPSM) was proposed in [17], where comprehensive performance comparisons were carried out between the GPSM scheme as well as the conventional MIMO scheme and the associated detection complexity issues were discussed. Furthermore, a range of practical issues were investigated, namely the detrimental effects of realistic imperfect Channel State Information at the Transmitter (CSIT), followed by a low-rank approximation invoked for large-dimensional MIMOs. Finally, the main difference between our GPSM scheme and the classic SM is that the former requires downlink pre-processing and CSIT, although they may be considered as a dual counterpart of each other and may hence be used in a hybrid manner. Other efforts on robust PSM was reported in [18].

Manuscript received March 17, 2014; revised June 2, 2014; accepted August 7, 2014. This work was supported by the EPSRC under the India-UK Advanced Technology Centre (IU-ATC), by the EU under the Concerto project, and by the European Research Council's (ERC) Advanced Fellow Grant. The associate editor coordinating the review of this paper and approving it for publication was M. Ardakani.

The authors are with the Communications, Signal Processing and Control, School of Electronics and Computer Science (ECS), University of Southampton, Southampton SO17 1BJ, U.K. (e-mail: rz@ecs.soton.ac.uk; lly@ecs.soton.ac.uk; lh@ecs.soton.ac.uk, <http://www-mobile.ecs.soton.ac.uk>).

Color versions of one or more of the figures in this paper are available online at <http://ieeexplore.ieee.org>.

Digital Object Identifier 10.1109/TWC.2014.2347297

As a further development, in this paper, we provide the theoretical analysis of the recently proposed GPSM scheme [17], which is not available in the literature. More explicitly, both the discrete-input continuous-output memoryless channel (DCMC) capacity as well as the achievable rate are characterized. Importantly, tight upper bounds of the symbol error ratio (SER) and bit error ratio (BER) expressions are derived, when a decoupled low-complexity detector is employed.

The rest of our paper is organised as follows. In Section II, we introduce the underlying concept as well as the detection methods of the GPSM scheme. This is followed by our analytical study in Section III, where both the DCMC capacity and the achievable rate as well as the SER/BER expressions are derived. Our simulation results are provided in Section IV, while we conclude in Section V.

II. SYSTEM MODEL

A. Conceptual Description

Consider a MIMO system equipped with N_t TAs and N_r RAs, where we assume $N_t \geq N_r$. In this MIMO set-up, a maximum of N_r parallel data streams may be supported, conveying a total of $k_{eff} = N_r k_{mod}$ bits altogether, where $k_{mod} = \log_2(M)$ denotes the number of bits per symbol of a conventional M -ary PSK/QAM scheme and its alphabet is denoted by \mathcal{A} . Transmitter Pre-Coding (TPC) relying on the TPC matrix of $\mathbf{P} \in \mathbb{C}^{N_t \times N_r}$ may be used for pre-processing the source signal before its transmission upon exploiting the knowledge of the CSIT.

In contrast to the above-mentioned classic multiplexing of N_r data streams, in our GPSM scheme a total of $N_a < N_r$ RAs are activated so as to facilitate the simultaneous transmission of N_a data streams, where the particular pattern of the N_a RAs activated conveys extra information in form of so-called spatial symbols in addition to the information carried by the conventional modulated symbols. Hence, the number of bits in GPSM conveyed by a spatial symbol becomes $k_{ant} = \lfloor \log_2(|\mathcal{C}_t|) \rfloor$, where the set \mathcal{C}_t contains all the combinations associated with choosing N_a activated RAs out of N_r RAs. As a result, the total number of bits transmitted by the GPSM scheme is $k_{eff} = k_{ant} + N_a k_{mod}$. Finally, it is plausible that the conventional MIMO scheme obeys $N_a = N_r$. For assisting further discussions, we also let $\mathcal{C}(k)$ and $\mathcal{C}(k, i)$ denote the k th RA activation pattern and the i th activated RA in the k th activation pattern, respectively.

B. GPSM Transmitter

More specifically, let \mathbf{s}_m^k be an explicit representation of a so-called super-symbol $\mathbf{s} \in \mathbb{C}^{N_r \times 1}$, indicating that the RA pattern k is activated and N_a conventional modulated symbols $\mathbf{b}_m = [b_{m1}, \dots, b_{mN_a}]^T \in \mathbb{C}^{N_a \times 1}$ are transmitted, where we have $b_{m_i} \in \mathcal{A}$ and $\mathbb{E}[|b_{m_i}|^2] = 1, \forall i \in [1, N_a]$. In other words, we have the relationship

$$\mathbf{s}_m^k = \mathbf{\Omega}_k \mathbf{b}_m, \quad (1)$$

where $\mathbf{\Omega}_k = \mathbf{I}[:, \mathcal{C}(k)]$ is constituted by the specifically selected columns determined by $\mathcal{C}(k)$ of an identity matrix of \mathbf{I}_{N_r} . Following TPC, the resultant transmit signal $\mathbf{x} \in \mathbb{C}^{N_t \times 1}$ may be written as

$$\mathbf{x} = \sqrt{\beta/N_a} \mathbf{P} \mathbf{s}_m^k. \quad (2)$$

To avoid dramatic power fluctuation during the pre-processing, we introduce the scaling factor of β designed for maintaining either the loose power-constraint of $\mathbb{E}[\|\mathbf{x}\|^2] = 1$ or the strict power-constraint of $\|\mathbf{x}\|^2 = 1$, which are thus denoted by β_l and β_s , respectively.

As a natural design, the TPC matrix has to ensure that no energy leaks into the unintended RA patterns. Hence, the classic linear Channel Inversion (CI)-based TPC [19], [20] may be used, which is formulated as

$$\mathbf{P} = \mathbf{H}^H (\mathbf{H} \mathbf{H}^H)^{-1} \quad (3)$$

where the power-normalisation factor of the output power after pre-processing is given by

$$\beta_l = \frac{N_r}{\text{Tr}[(\mathbf{H} \mathbf{H}^H)^{-1}]}, \quad (4)$$

$$\beta_s = \frac{N_a}{\mathbf{s}^H (\mathbf{H} \mathbf{H}^H)^{-1} \mathbf{s}}. \quad (5)$$

The stringent power-constraint of (5) is less common than the loose power-constraint of (4). The former prevents any of the power fluctuations at the transmitter, which was also considered in [19]. For completeness, we include both power-constraints in this paper.

C. GPSM Receiver

The signal observed at the N_r RAs may be written as

$$\mathbf{y} = \sqrt{\beta/N_a} \mathbf{H} \mathbf{P} \mathbf{s}_m^k + \mathbf{w}, \quad (6)$$

where $\mathbf{w} \in \mathbb{C}^{N_r \times 1}$ is the circularly symmetric complex Gaussian noise vector with each entry having a zero mean and a variance of σ^2 , i.e. we have $\mathbb{E}[\|\mathbf{w}\|^2] = \sigma^2 \mathbf{I}_{N_r}$, while $\mathbf{H} \in \mathbb{C}^{N_r \times N_t}$ represents the MIMO channel involved. We assume furthermore that each entry of \mathbf{H} undergoes frequency-flat Rayleigh fading and it is uncorrelated between different super-symbol transmissions, while remains constant within the duration of a super-symbol's transmission. The super-symbols transmitted are statistically independent from the noise.

At the receiver, the joint detection of both the conventional modulated symbols \mathbf{b}_m and of the spatial symbol k obeys the Maximum Likelihood (ML) criterion, which is formulated as

$$[\hat{m}_1, \dots, \hat{m}_{N_a}, \hat{k}] = \arg \min_{\mathbf{s}_n^\ell \in \mathcal{B}} \left\{ \left\| \mathbf{y} - \sqrt{\beta/N_a} \mathbf{H} \mathbf{P} \mathbf{s}_n^\ell \right\|^2 \right\}, \quad (7)$$

where $\mathcal{B} = \mathcal{C} \times \mathcal{A}^{N_a}$ is the joint search space of the super-symbol \mathbf{s}_n^ℓ . Alternatively, decoupled or separate detection may also be employed, which treats the detection of the conventional

172 modulated symbols \mathbf{b}_m and the spatial symbol k separately. In
173 this reduced-complexity variant,¹ we have

$$\begin{aligned}\hat{k} &= \arg \max_{\ell \in [1, |\mathcal{C}|]} \left\{ \sum_{i=1}^{N_a} |y_{\mathcal{C}(\ell, i)}|^2 \right\}, \\ \hat{m}_i &= \arg \min_{n_i \in [1, M]} \left\{ \left| y_{\hat{v}_i} - \sqrt{\beta/N_a} \mathbf{h}_{\hat{v}_i} \mathbf{p}_{\hat{v}_i} b_{n_i} \right|^2 \right\}_{\hat{v}_i = \mathcal{C}(\hat{k}, i)},\end{aligned}\quad (8)$$

174 where $\mathbf{h}_{\hat{v}_i}$ is the \hat{v}_i th row of \mathbf{H} representing the channel
175 between the \hat{v}_i th RA and the transmitter, while $\mathbf{p}_{\hat{v}_i}$ is the \hat{v}_i th
176 column of \mathbf{P} representing the \hat{v}_i th TPC vector. Thus, correct
177 detection is declared, when we have $\hat{k} = k$ and $\hat{m}_i = m_i$, $\forall i$.

178 *Remarks:* Note that the complexity of the ML detection of
179 (7) is quite high, which is on the order determined by the
180 super-alphabet \mathcal{B} , hence obeying $\mathcal{O}(|\mathcal{C}|M^{N_a})$. By contrast, the
181 decoupled detection of (8) and (9) facilitates a substantially
182 reduced complexity compared to that of (7). More explicitly, the
183 complexity is imposed by detecting N_a conventional modulated
184 symbols, plus the complexity (κ) imposed by the comparisons
185 invoked for non-coherently detecting the spatial symbol of (8),
186 which may be written as $\mathcal{O}(N_a M + \kappa)$. Further discussions
187 about the detection complexity of the decoupled detection of
188 the GPSM scheme may be found in [17], where the main
189 conclusion is that the complexity of the decoupled detection
190 of the GPSM scheme is no higher than that of the conventional
191 MIMO scheme corresponding to $N_a = N_r$.

192 III. PERFORMANCE ANALYSIS

193 We continue by investigating the DCMC capacity of our
194 GPSM scheme, when the joint detection scheme of (7) is
195 used and then quantify its achievable rate, when the realistic
196 decoupled detection of (8) and (9) is employed. The achievable
197 rate expression requires the theoretical BER/SER analysis of
198 the GPSM scheme, which provides more insights into the inner
199 nature of our GPSM scheme.²

200 A. DCMC Capacity and Achievable Rate

201 Both Shannon's channel capacity and its MIMO generalisa-
202 tion are maximized, when the input signal obeys a Gaussian
203 distribution [22]. Our GPSM scheme is special in the sense that
204 the spatial symbol conveys integer values constituted by the RA

¹The reduced complexity receiver operates in a decoupled manner, which is beneficial in the scenario considered, where the spatial symbols and the conventionally modulated symbols are independent. However, this assumption may not be ideal, when correlations exist between the spatial symbols and the conventionally modulated symbols. In this case, an iterative detection exchanging extrinsic soft-information between the spatial symbols and conventionally modulated symbols may be invoked. Importantly, the iterations would exploit the beneficial effects of improving the soft-information by taking channel decoding into account as well for simultaneously exploiting the underlying correlations, which is reminiscent of the detection of correlated source. A further inspiration would be to beneficially map the symbols to both the spatial and to the conventional domain at the transmitter, so that the benefits of unequal protection could be exploited.

²The Pair-wise Error Probability (PEP) analysis, relying on error events [21], was conducted in our previous contribution for the specific scenario of ML based detection [17]. In this paper, our error probability analysis is dedicated to the low-complexity decoupled detection philosophy

pattern index, which does not obey the shaping requirements of 205 Gaussian signalling. This implies that the channel capacity of 206 the GPSM scheme depends on a mixture of a continuous and 207 a discrete input. Hence, for simplicity's sake, we discuss the 208 DCMC capacity and the achievable rate of our GPSM scheme 209 in the context of discrete-input signalling for both the spatial 210 symbol and for the conventional modulated symbols mapped 211 to it. 212

1) *DCMC Capacity:* Upon recalling the received signal ob- 213 served at the N_r RAs expressed in (6), the conditional probabil- 214 ity of receiving \mathbf{y} given that a $\mathcal{M} = |\mathcal{C}|M^{N_a}$ -ary super-symbol 215 $\mathbf{s}_\tau \in \mathcal{B}$ was transmitted over Rayleigh channel and subjected to 216 the TPC of (3) is formulated as 217

$$p(\mathbf{y}|\mathbf{s}_\tau) = \frac{1}{\pi\sigma^2} \exp \left\{ -\frac{\|\mathbf{y} - \mathbf{G}\mathbf{s}_\tau\|^2}{\sigma^2} \right\}, \quad (10)$$

where $\mathbf{G} = \sqrt{\beta/N_a} \mathbf{H} \mathbf{P}$. The DCMC capacity of the ML- 218 based joint detection of our GPSM scheme is given by [23] 219

$$C = \max_{p(\mathbf{s}_1), \dots, p(\mathbf{s}_M)} \sum_{\tau=1}^M \int_{-\infty}^{\infty} p(\mathbf{y}, \mathbf{s}_\tau) \log_2 \left(\frac{p(\mathbf{y}|\mathbf{s}_\tau)}{\sum_{\epsilon=1}^M p(\mathbf{y}, \mathbf{s}_\epsilon)} \right) d\mathbf{y}, \quad (11)$$

which is maximized, when we have $p(\mathbf{s}_\tau) = 1/M$, $\forall \tau$ [23]. 220 Furthermore, we have 221

$$\begin{aligned}\log_2 \left(\frac{p(\mathbf{y}|\mathbf{s}_\tau)}{\sum_{\epsilon=1}^M p(\mathbf{y}, \mathbf{s}_\epsilon)} \right) &= \log_2 \left(\frac{p(\mathbf{y}|\mathbf{s}_\tau)}{\sum_{\epsilon=1}^M p(\mathbf{y}|\mathbf{s}_\epsilon)p(\mathbf{s}_\epsilon)} \right) \\ &= -\log_2 \left(\frac{1}{M} \sum_{\epsilon=1}^M \frac{p(\mathbf{y}|\mathbf{s}_\epsilon)}{p(\mathbf{y}|\mathbf{s}_\tau)} \right) \\ &= \log_2(M) - \log_2 \sum_{\epsilon=1}^M \exp(\Psi),\end{aligned}\quad (12)$$

where substituting (10) into (12), the term Ψ is expressed as 222

$$\Psi = \frac{-\|\mathbf{G}(\mathbf{s}_\tau - \mathbf{s}_\epsilon) + \mathbf{w}\|^2 + \|\mathbf{w}\|^2}{\sigma^2}. \quad (13)$$

Finally, by substituting (12) into (11) and exploiting that $p(\mathbf{s}_\tau) = 223$ $1/M$, $\forall \tau$, we have 224

$$C = \log_2(M) - \frac{1}{M} \sum_{\tau=1}^M \mathbb{E}_{\mathbf{G}, \mathbf{w}} \left[\log_2 \sum_{\epsilon=1}^M \exp(\Psi) \right]. \quad (14)$$

2) *Achievable Rate:* The above DCMC capacity expression 225 implicitly relies on the ML-based joint detection of (7), which 226 has a complexity on the order of $\mathcal{O}(M)$. When the reduced- 227 complexity decoupled detection of (8) and (9) is employed, we 228 estimate the achievable rate based on the mutual information 229 $I(z; \hat{z})$ per bit measured for our GPSM scheme between the 230 input bits $z \in [0, 1]$ and the corresponding demodulated output 231 bits $\hat{z} \in [0, 1]$. 232

The mutual information per bit $I(z; \hat{z})$ is given for the Binary 233 Symmetric Channel (BSC) by [22]: 234

$$I(z; \hat{z}) = H(z) - H(z|\hat{z}), \quad (15)$$

where $H(z) = -\sum_z P_z \log_2 P_z$ represents the entropy of the input bits z and P_z is the Probability Mass Function (PMF) of z . It is noted furthermore that we have $H(z) = 1$, when we adopt the common assumption of equal-probability bits, i.e. $P_{z=0} = P_{z=1} = 1/2$. On the other hand, the conditional entropy $H(z|\hat{z})$ represents the average uncertainty about z after observing \hat{z} , which is given by:

$$H(z|\hat{z}) = \sum_{\hat{z}} P_{\hat{z}} \left[\sum_z P_{z|\hat{z}} \log_2 P_{z|\hat{z}} \right] = -e_x \log_2 e_x - (1 - e_x) \log_2 (1 - e_x), \quad (16)$$

where e_x is the crossover probability. By substituting (16) into (15) and exploiting $H(z) = 1$ we have:

$$I(z; \hat{z}) = 1 + e_x \log_2 e_x + (1 - e_x) \log_2 (1 - e_x). \quad (17)$$

Since the input bit in our GPSM scheme may be mapped either to a spatial symbol or to a conventional modulated symbol with a probability of k_{ant}/k_{eff} and $N_a k_{mod}/k_{eff}$, respectively, the achievable rate becomes

$$R = k_{ant} I(e_x = e_{ant}^b) + N_a k_{mod} I(e_x = \tilde{e}_{mod}^b), \quad (18)$$

where e_{ant}^b represents the BER of the spatial symbol, while \tilde{e}_{mod}^b represents the BER of the conventional modulated symbols in the presence of spatial symbol errors due to the detection of (8).

B. Error Probability

1) *The Expression of e_{eff}^s and e_{eff}^b* : Let us first let e_{ant}^s represent the SER of the spatial symbol, while \tilde{e}_{mod}^s represent the SER of the conventional modulated symbols in the presence of spatial symbol errors. Let further N_{ant}^e and N_{mod}^e represent the number of symbol errors in the spatial symbols and in the conventional modulated symbols, respectively. Then we have $e_{ant}^s = N_{ant}^e/N_s$ and $\tilde{e}_{mod}^s = N_{mod}^e/N_a N_s$, where N_s is the total number of GPSM symbols. Hence, the average SER e_{eff}^s of our GPSM scheme is given by:

$$e_{eff}^s = \frac{(N_{ant}^e + N_{mod}^e)}{(1 + N_a)N_s} = \frac{(e_{ant}^s + N_a \tilde{e}_{mod}^s)}{(1 + N_a)}. \quad (19)$$

Similarly, the average BER e_{eff}^b of our GPSM scheme may be written as:

$$e_{eff}^b = \frac{(k_{ant} e_{ant}^b + N_a k_{mod} \tilde{e}_{mod}^b)}{k_{eff}} \approx \frac{(\delta_{ant} e_{ant}^s + N_a \tilde{e}_{mod}^s)}{k_{eff}}. \quad (20)$$

where the second equation of (20) follows from the relation

$$\tilde{e}_{mod}^b \approx \frac{\tilde{e}_{mod}^s}{k_{mod}}, \quad (21)$$

$$e_{ant}^b \approx \frac{\delta_{ant} e_{ant}^s}{k_{ant}}. \quad (22)$$

Importantly, we have Lemma III.1 for the expression of $\delta_{k_{ant}}$ acting as a correction factor in (22).

Lemma III.1. (Proof in Appendix A): The generic expression of the correction factor $\delta_{k_{ant}}$ for k_{ant} bits of information is given by:

$$\delta_{k_{ant}} = \delta_{k_{ant}-1} + \frac{2^{k_{ant}-1} - \delta_{k_{ant}-1}}{2^{k_{ant}} - 1}, \quad (23)$$

where given $\delta_0 = 0$, we can recursively determine $\delta_{k_{ant}}$.

Furthermore, by considering (21) and (22), the achievable rate expressed in (18) may be written as

$$R \approx k_{ant} I\left(\frac{\delta_{k_{ant}} e_{ant}^s}{k_{ant}}\right) + N_a k_{mod} I\left(\frac{\tilde{e}_{mod}^s}{k_{mod}}\right). \quad (24)$$

Hence, as suggested by (19), (20) and (24), we find that both the average error probability as well as the achievable rate of our GPSM scheme requires the entries of e_{ant}^s and \tilde{e}_{mod}^s , which will be discussed as follows.

2) *Upper Bound of e_{ant}^s* : We commence our discussion by directly formulating the following lemma:

Lemma III.2. (Proof in Appendix B): The upper bound of the analytical SER of the spatial symbol of our GPSM scheme relying on CI TPC may be formulated as:

$$e_{ant}^s \leq e_{ant}^{s,ub} = 1 - \int_0^\infty \left\{ \int_0^\infty [F_{\chi_2^2}(g)]^{N_r - N_a} f_{\chi_2^2}(g; \lambda) dg \right\}^{N_a} f_\lambda(\lambda) d\lambda, \quad (25)$$

where $F_{\chi_2^2}(g)$ represents the Cumulative Distribution Function (CDF) of a chi-square distribution having two degrees of freedom, while $f_{\chi_2^2}(g; \lambda)$ represents the Probability Distribution Function (PDF) of a non-central chi-square distribution having two degrees of freedom and non-centrality given by

$$\lambda = \frac{\beta}{N_a \sigma_0^2}, \quad (26)$$

with its PDF of $f_\lambda(\lambda)$ and $\sigma_0^2 = \sigma^2/2$. Finally, equality of (25) holds when $N_a = 1$.

Moreover, the PDF of $f_\lambda(\lambda)$ is formulated in Lemma III.3 and Lemma III.4, respectively, when either the loose or stringent power-normalisation factor of (4) and (5) is employed.

Lemma III.3 (Proof in Appendix C): When CI TPC is employed and the loose power-normalisation factor of (4) is used, the distribution $f_\lambda(\lambda)$ of the non-centrality λ is given by:

$$f_\lambda(\lambda) = \frac{2N_r}{\lambda^2 N_a \sigma^2} f_U\left(\frac{2N_r}{\lambda N_a \sigma^2}\right), \quad (27)$$

where by letting $U = \text{Tr}[(\mathbf{H}\mathbf{H}^H)^{-1}]$, we have $f_U(\cdot)$, which constitutes the derivative of $F_U(\cdot)$ and it is given in (50) of Appendix C.

Lemma III.4. (Proof in Appendix D): When CI TPC is employed and the stringent power-normalisation factor of (5) is used, the distribution $f_\lambda(\lambda)$ of the non-centrality λ is given by:

$$f_\lambda(\lambda) = \frac{N_a^{N_t - N_r + 1} \sigma^2 / 2}{(N_t - N_r)!} e^{-\lambda N_a \sigma^2 / 2} \left(\frac{\lambda \sigma^2}{2}\right)^{N_t - N_r}. \quad (28)$$

301 3) *Upper Bound of \tilde{e}_{mod}^s* : Considering a general case of
 302 N_r as well as N_a and assuming that the RA pattern $\mathcal{C}(k)$ was
 303 activated, after substituting (3) into (6), we have:

$$y_{v_i} = \sqrt{\beta/N_a} b_{m_i} + w_{v_i}, \quad \forall v_i \in \mathcal{C}(k), \quad (29)$$

$$y_{u_i} = w_{u_i}, \quad \forall u_i \in \bar{\mathcal{C}}(k), \quad (30)$$

304 where $\bar{\mathcal{C}}(k)$ denotes the complementary set of the activated RA
 305 pattern $\mathcal{C}(k)$ in \mathcal{C} . Hence, we have the signal to noise ratio
 306 (SNR) given as

$$\gamma = \gamma_{v_i} = \frac{\beta}{N_a \sigma^2} = \frac{\lambda}{2}, \quad \forall v_i \quad (31)$$

307 and for the remaining deactivated RAs in $\bar{\mathcal{C}}(k)$, we have only
 308 random noises of zero mean and variance of σ^2 .

309 The SER e_{mod}^s of the conventional modulated symbol $b_{m_i} \in$
 310 \mathcal{A} in the *absence* of spatial symbol errors may be upper
 311 bounded by [24]:

$$e_{\text{mod}}^s < N_{\min} \int_0^\infty \mathcal{Q}(d_{\min} \sqrt{\gamma/2}) f_\gamma(\gamma) d\gamma = e_{\text{mod}}^{s,ub}, \quad (32)$$

312 where in general $f_\gamma(\gamma)$ has to be acquired by the empirical
 313 histogram based method. When Lemma III.3 or Lemma III.4
 314 is exploited, $f_\gamma(\gamma)$ is a scaled version of $f_\lambda(\lambda)$, i.e. we have
 315 $f_\gamma(\gamma) = 2f_\lambda(2\gamma)$. Moreover, d_{\min} is the minimum Euclidean
 316 distance in the conventional modulated symbol constellation,
 317 N_{\min} is the average number of the nearest neighbours separated
 318 by d_{\min} in the constellation and $\mathcal{Q}(\cdot)$ denotes the Gaussian
 319 \mathcal{Q} -function.

320 When taking into account of the spatial symbol errors, we
 321 have Lemma III.5 for the upper bound of \tilde{e}_{mod}^s .

322 *Lemma III.5. (Proof in Appendix E)*: Given the k th activated
 323 RA patten, the SER of the conventional modulated symbols in
 324 the *presence* of spatial symbol errors can be upper bounded by:

$$\begin{aligned} \tilde{e}_{\text{mod}}^s &< \left(1 - e_{\text{ant}}^{s,ub}\right) e_{\text{mod}}^{s,ub} \\ &+ e_{\text{ant}}^{s,ub} \sum_{\ell \neq k} \frac{N_c e_{\text{mod}}^{s,ub} + N_d e_o^s}{N_a (2^{k_{\text{ant}}} - 1)} = \tilde{e}_{\text{mod}}^{s,ub}, \end{aligned} \quad (33)$$

325 where N_c and $N_d = (N_a - N_c)$ represent the number of com-
 326 mon and different RA between $\mathcal{C}(\ell)$ and $\mathcal{C}(k)$, respectively.
 327 Mathematically we have $N_c = \sum_{i=1}^{N_a} \mathbb{I}[\mathcal{C}(\ell, i) \in \mathcal{C}(k)]$. More-
 328 over, $e_o^s = (M - 1)/M$ is SER as a result of random guess.

329 4) *Upper Bound of e_{eff}^s and e_{eff}^b* : By substituting (25) and
 330 (33) into (19) and (20), we arrive at the upper bound of the
 331 average symbol and bit error probability as

$$e_{\text{eff}}^{s,ub} = \frac{(e_{\text{ant}}^{s,ub} + N_a \tilde{e}_{\text{mod}}^{s,ub})}{(1 + N_a)} \quad (34)$$

$$e_{\text{eff}}^{b,ub} = \frac{(\delta_{\text{ant}} e_{\text{ant}}^{s,ub} + N_a \tilde{e}_{\text{mod}}^{s,ub})}{k_{\text{eff}}}. \quad (35)$$

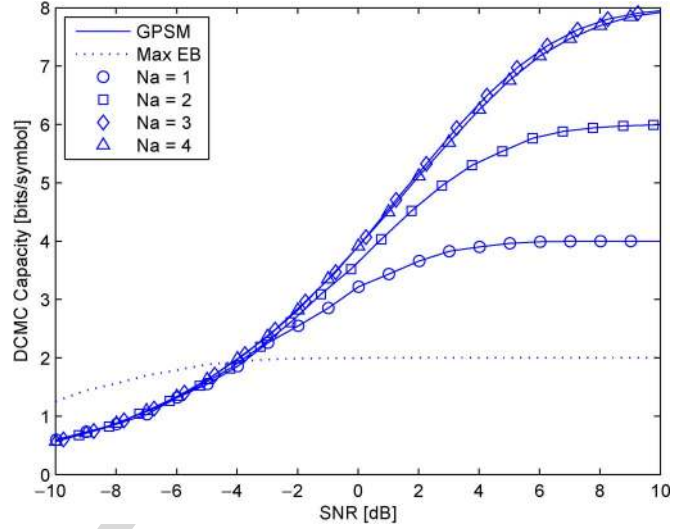


Fig. 1. DCMC capacity versus the SNR of the CI TPC aided GPSM scheme based on the loose power-normalisation factor of (4) under $\{N_t, N_r\} = \{8, 4\}$ and employing QPSK, while having $N_a = \{1, 2, 3, 4\}$ activated RAs.

Similarly, by substituting (25) and (33) into (24), we obtain the
 lower bound of the achievable rate as

$$R^{lb} = k_{\text{ant}} I \left(\delta_{k_{\text{ant}}} \frac{e_{\text{ant}}^{s,ub}}{k_{\text{ant}}} \right) + N_a k_{\text{mod}} I \left(\frac{\tilde{e}_{\text{mod}}^{s,ub}}{k_{\text{mod}}} \right). \quad (36)$$

IV. NUMERICAL RESULTS

We now provide numerical results for characterizing both the
 DCMC capacity of our GPSM scheme and for demonstrating
 the accuracy of our analytical error probability results.

A. DCMC Capacity

1) *Effect of the Number of Activated RAs*: Fig. 1 charac-
 terises the DCMC capacity versus the SNR of the CI TPC
 aided GPSM scheme based on the loose power-normalisation
 factor of (4) under $\{N_t, N_r\} = \{8, 4\}$ and employing QPSK,
 while having $N_a = \{1, 2, 3, 4\}$ activated RAs. It can be ob-
 served in Fig. 1 that the larger N_a , the higher the capacity of
 our GPSM scheme. Importantly, both the GPSM scheme of
 $N_a = 3$ marked by the diamonds and its conventional MIMO
 counterpart of $N_a = 4$ marked by the triangles attain the same
 ultimate DCMC capacity of 8 bits/symbol at a sufficiently high
 SNR, albeit the former exhibits a slightly higher capacity before
 reaching the 8 bits/symbol value. Furthermore, the DCMC ca-
 pacity of the conventional Maximal Eigen-Beamforming (Max
 EB) scheme is also included as a benchmark under $\{N_t, N_r\} =$
 $\{8, 4\}$ and employing QPSK, which exhibits a higher DCMC
 capacity at low SNRs, while only supporting 2 bits/symbol
 at most.

We further investigate the attainable bandwidth efficiency by
 replacing the SNR used in Fig. 1 by the SNR per bit in Fig. 2,
 where we have $\text{SNR}_b[\text{dB}] = \text{SNR}[\text{dB}] - 10 \log_{10}(C/N_a)$. It
 can be seen from Fig. 2 that the lower N_a , the higher the
 bandwidth efficiency attained in the low range of SNR_b . Im-
 portantly, the achievable bandwidth efficiency of $N_a = 3$ is

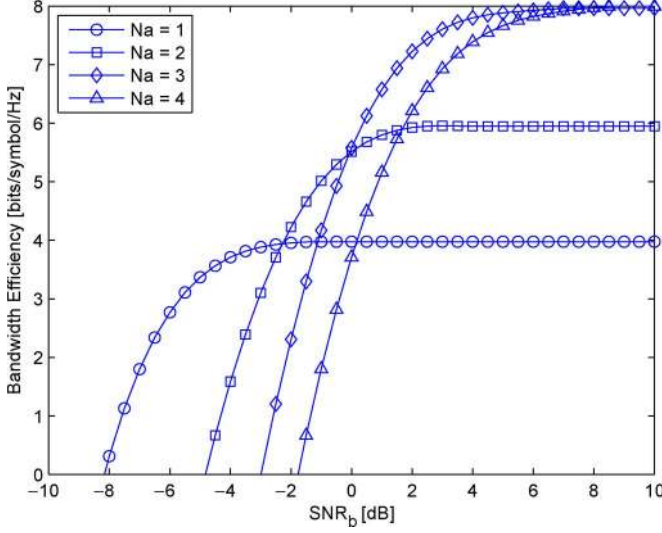


Fig. 2. Bandwidth efficiency versus the SNR_b of CI TPC aided GPSM scheme with the loose power-normalisation factor of (4) under $\{N_t, N_r\} = \{8, 4\}$ and employing QPSK, while having $N_a = \{1, 2, 3, 4\}$ activated RAs.

consistently and significantly higher than that achieved by $N_a = 4$, before they both converge to 8 bits/symbol/Hz at their maximum. Overall, there is always a beneficial configuration for our GPSM scheme that offers the same bandwidth efficiency as that of its conventional MIMO counterpart, which is achieved at a lower SNR per bit.

2) *Robustness to Impairments*: Like in all TPC schemes, an important aspect related to GPSM is its resilience to CSIT inaccuracies. In this paper, we let $\mathbf{H} = \mathbf{H}_a + \mathbf{H}_i$, where \mathbf{H}_a represents the matrix hosting the average CSI, with each entry obeying the complex Gaussian distribution of $h_a \sim \mathcal{CN}(0, \sigma_a^2)$ and \mathbf{H}_i is the instantaneous CSI error matrix obeying the complex Gaussian distribution of $h_i \sim \mathcal{CN}(0, \sigma_i^2)$, where we have $\sigma_a^2 + \sigma_i^2 = 1$. As a result, only \mathbf{H}_a is available at the transmitter for pre-processing.

Another typical impairment is antenna correlation. The correlated MIMO channel is modelled by the widely-used Kronecker model, which is written as $\mathbf{H} = (\mathbf{R}_t^{1/2})\mathbf{G}(\mathbf{R}_r^{1/2})^T$, with \mathbf{G} representing the original MIMO channel imposing no correlation, while \mathbf{R}_t and \mathbf{R}_r represents the correlations at the transmitter and receiver side, respectively, with the correlation entries given by $R_t(i, j) = \rho_t^{|i-j|}$ and $R_r(i, j) = \rho_r^{|i-j|}$.

Figs. 3 and 4 characterise the effect of imperfect CSIT associated with $\sigma_i = 0.4$ and of antenna correlation of $\rho_t = \rho_r = 0.3$ on the attainable DCMC capacity versus the SNR for our CI TPC aided GPSM scheme with the loose power-normalisation factor of (4), respectively, under $\{N_t, N_r\} = \{8, 4\}$ and employing QPSK having $N_a = \{1, 2, 3, 4\}$ activated RAs. It can be seen that as expected, both impairments result into a degraded DCMC capacity. Observe in Fig. 3 for imperfect CSIT that the degradation of the conventional MIMO associated with $N_a = 4$ and marked by the triangle is larger than that of our GPSM scheme corresponding $N_a = \{1, 2, 3\}$. On the other hand, as seen in Fig. 4, roughly the same level of degradation is observed owing to antenna correlation.

3) *Effect of Modulation Order and MIMO Configuration*: Fig. 5 characterises the DCMC capacity versus the SNR

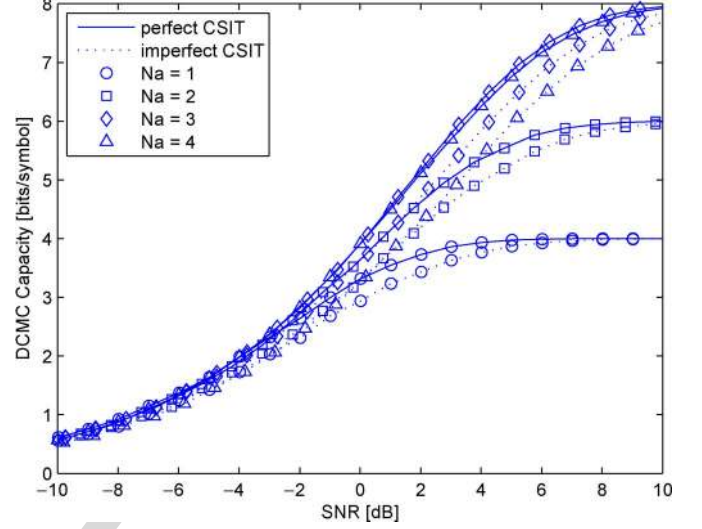


Fig. 3. The effect of imperfect CSIT with $\sigma_i = 0.4$ on the DCMC capacity versus the SNR of CI TPC aided GPSM scheme with the loose power-normalisation factor of (4) under $\{N_t, N_r\} = \{8, 4\}$ and employing QPSK having $N_a = \{1, 2, 3, 4\}$ activated RAs.

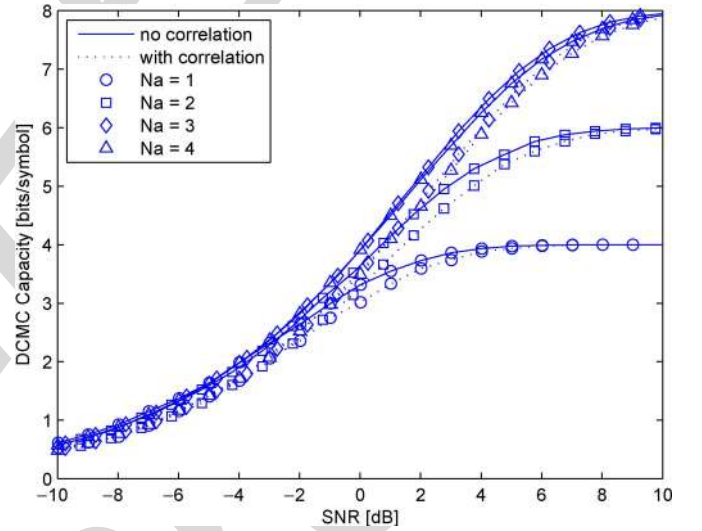


Fig. 4. The effect of antenna correlation with $\rho_t = \rho_r = 0.3$ on the DCMC capacity versus the SNR of CI TPC aided GPSM scheme with the loose power-normalisation factor of (4) under $\{N_t, N_r\} = \{8, 4\}$ and employing QPSK having $N_a = \{1, 2, 3, 4\}$ activated RAs.

of our CI TPC aided GPSM scheme relying on the loose power-normalisation factor of (4) under $\{N_t, N_r\} = \{8, 4\}$ and employing various conventional modulation schemes having $N_a = \{1, 2\}$ activated RAs. It can be seen that the higher the modulation order M , the higher the achievable DCMC capacity. Furthermore, for a fixed modulation order M , the higher the value of N_a , the higher the achievable DCMC capacity becomes as a result of the information embedded in the spatial symbol.

Fig. 6 characterises the DCMC capacity versus the SNR for our CI TPC aided GPSM scheme for the loose power-normalisation factor of (4) under different settings of $\{N_t, N_r\}$ with $N_t/N_r = 2$ and employing QPSK, while having $N_a = \{1, 2\}$ activated RAs. It can be seen in Fig. 6 that for a fixed MIMO setting, the higher the value of N_a , the higher the

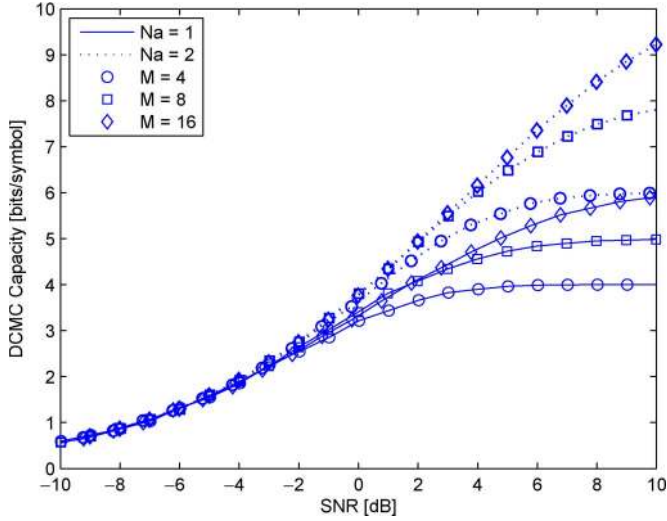


Fig. 5. DCMC capacity versus the SNR of our CI TPC aided GPSM scheme relying on the loose power-normalisation factor of (4) under $\{N_t, N_r\} = \{8, 4\}$ and employing various conventional modulation schemes having $N_a = \{1, 2\}$ activated RAs.

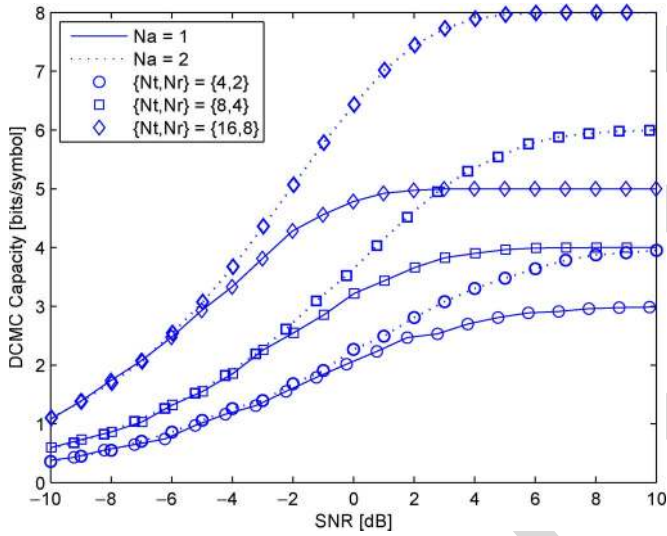


Fig. 6. DCMC capacity versus the SNR for our CI TPC aided GPSM scheme for the loose power-normalisation factor of (4) under different settings of $\{N_t, N_r\}$ with $N_t/N_r = 2$ and employing QPSK, while having $N_a = \{1, 2\}$ activated RAs.

414 DCMC capacity becomes. Importantly, for a fixed N_a , the
415 larger the size of the MIMO antenna configuration, the higher
416 the DCMC capacity.

417 B. Achievable Rate

418 1) *Error Probability*: Figs. 7–10 characterize the GPSM
419 scheme's SER as well as the BER under both the loose
420 power-normalisation factor of (4) and the stringent power-
421 normalisation factor of (5) for $\{N_t, N_r\} = \{16, 8\}$ and em-
422 ploying QPSK, respectively. From Figs. 7–10, we recorded the
423 curves from left to right corresponding to $N_a = \{1, 2, 4, 6\}$. For
424 reasons of space-economy and to avoid crowded figures, our
425 results for $N_a = \{3, 5, 7\}$ were not shown here, but they obey
426 the same trends.

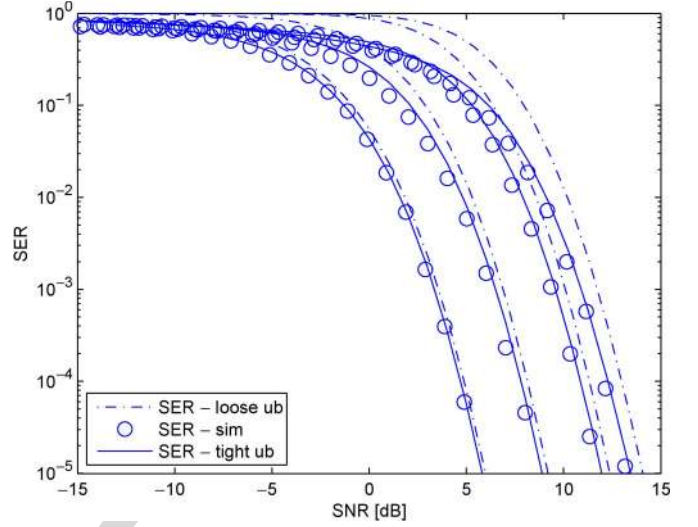


Fig. 7. GPSM scheme's SER with CI TPC and the **loose** power-normalisation factor of (4) under $\{N_t, N_r\} = \{16, 8\}$ and employing QPSK. Curves from left to right correspond to $N_a = \{1, 2, 4, 6\}$.

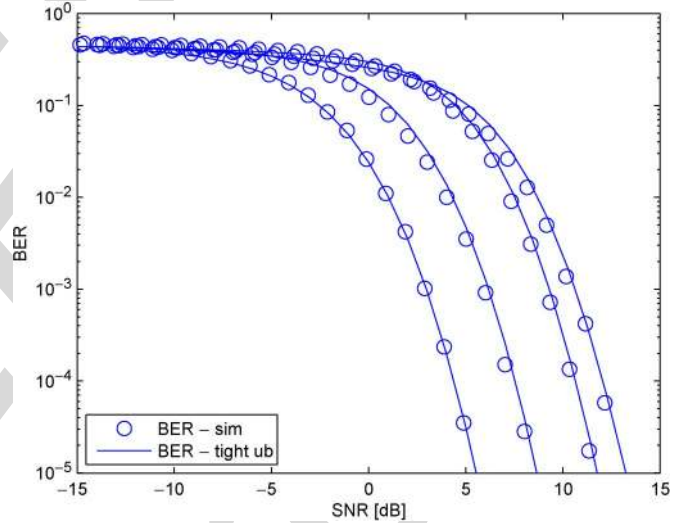


Fig. 8. GPSM scheme's BER with CI TPC and the **loose** power-normalisation factor of (4) under $\{N_t, N_r\} = \{16, 8\}$ and employing QPSK. Curves from left to right correspond to $\{N_a = 1, 2, 4, 6\}$.

It can be seen from Figs. 7 and 9 that our analytical SER
results of (34) form tight upper bounds for the empirical sim-
ulation results. Hence they are explicitly referred to as 'tight
upper bound' in both figures. Additionally, a loose upper bound
of the GPSM scheme's SER is also included, which may be
written as

$$e_{eff}^{s, lub} = 1 - \left(1 - e_{ant}^{s, ub}\right) \left(1 - e_{mod}^{s, ub}\right). \quad (37)$$

Note that in this loose upper bound expression, $e_{mod}^{s, ub}$ of (32) is
required rather than $\tilde{e}_{mod}^{s, ub}$ of (33). This expression implicitly
assumes that the detection of (8) and (9) are independent.
However, the first-step detection of (8) significantly affects the
second-step detection of (9). Hence, the loose upper bound
shown by the dash-dot line is only tight for $N_a = 1$ and
becomes much looser upon increasing N_a , when compared to
the tight upper bound of (34).

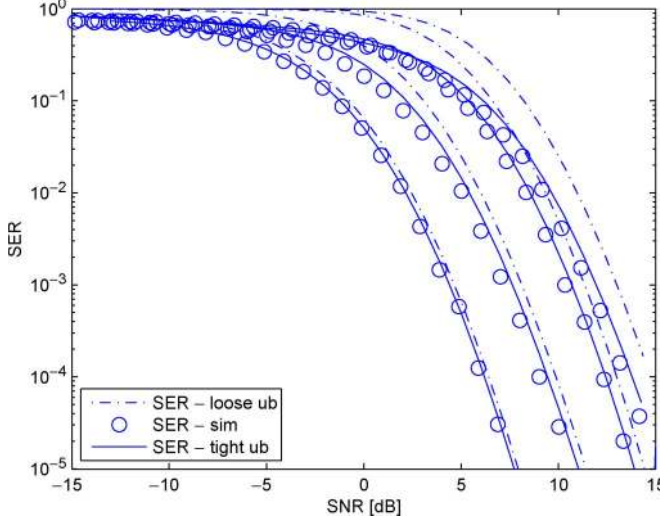


Fig. 9. GPSM scheme's SER with CI TPC and the **stringent** power-normalisation factor of (5) under $\{N_t, N_r\} = \{16, 8\}$ and employing QPSK. Curves from left to right correspond to $N_a = \{1, 2, 4, 6\}$.

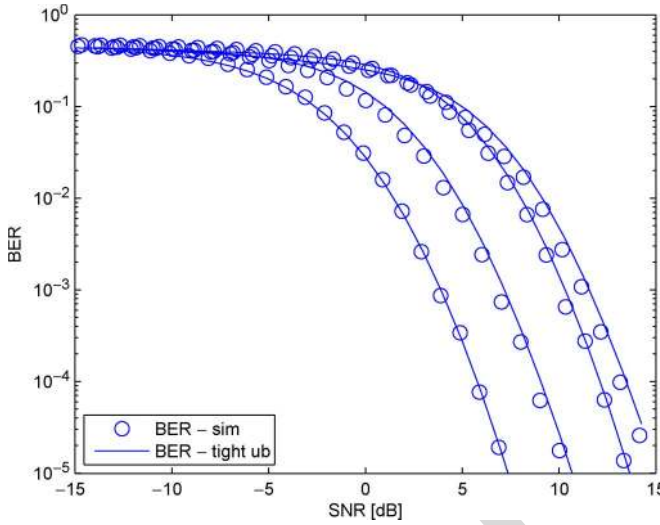


Fig. 10. GPSM scheme's BER with CI TPC and the **stringent** power-normalisation factor of (5) under $\{N_t, N_r\} = \{16, 8\}$ and employing QPSK. Curves from left to right correspond to $\{N_a = 1, 2, 4, 6\}$.

441 Similarly, when the GPSM scheme's BER is considered in
442 Figs. 8 and 10, our the analytical results of (35) again form
443 tight upper bounds for the empirical results.

444 2) *Separability*: To access the inner nature of first-step de-
445 tection of (8), Fig. 11 reveals the separability between the
446 activated RAs and deactivated RAs in our GPSM scheme,
447 where the PDF of (44) and (45) were recorded both for SNR =
448 -5 dB (left subplot) and for SNR = 0 dB (right subplot)
449 respectively for the same snapshot of MIMO channel realisation
450 with the aid of CI TPC and the loose power-normalisation factor
451 of (4) under $\{N_t, N_r\} = \{16, 8\}$ and employing QPSK. By
452 comparing the left subplot to the right subplot, it becomes clear
453 that the higher the SNR, the better the separability between the
454 activated and the deactivated RAs, since the mean of the solid
455 curves representing (44) move further apart from that of the
456 dashed curve representing (45). Furthermore, as expected, the

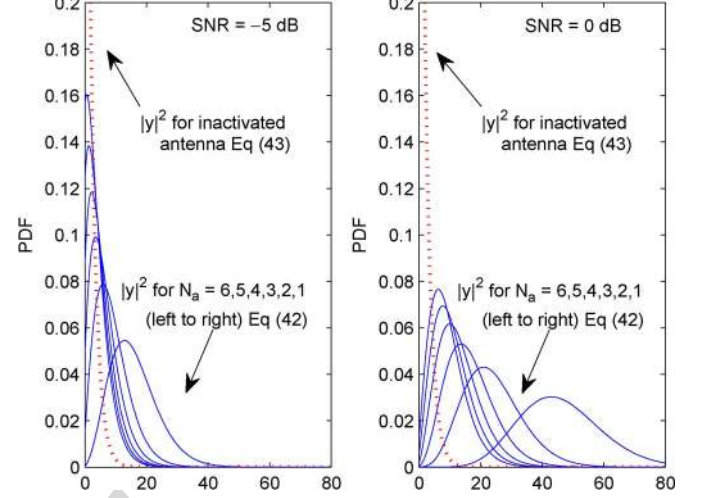


Fig. 11. The PDF of (44) and (45) under both SNR = -5 dB (left) and SNR = 0 dB (right) for the same snapshot of MIMO channel realisation with CI TPC and the loose power-normalisation factor of (4) under $\{N_t, N_r\} = \{16, 8\}$ and employing QPSK.

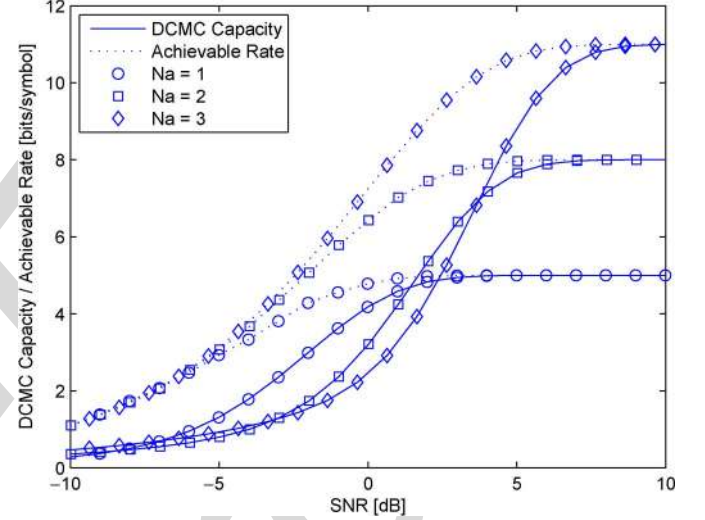


Fig. 12. Comparison between the DCMC capacity of our GPSM scheme relying implicitly on the ML-based joint detection and its lower bound of the achievable rate relying on the low-complexity decoupled detection, where we use CI TPC with the loose power-normalisation factor of (4) under $\{N_t, N_r\} = \{16, 8\}$ and employing QPSK having $N_a = \{1, 2, 3\}$.

457 lower N_a , the better the separability becomes, as demonstrated
458 in both subplots of Fig. 11.

459 3) *Comparison*: Finally, Fig. 12 characterizes the compar-
460 ison between the DCMC capacity (14) of our GPSM scheme
461 relying implicitly on the ML-based joint detection of (7) and
462 its lower bound of the achievable rate in (36) relying on the
463 low-complexity decoupled detection of (8) and (9), where we
464 use CI TPC with the loose power-normalisation factor of (4)
465 under $\{N_t, N_r\} = \{16, 8\}$ and employing QPSK having $N_a =$
466 $\{1, 2, 3\}$.

467 It is clear that the DCMC capacity is higher than the
468 achievable rate for each N_a considered, although both of them
469 converge to the same value, when the SNR is sufficiently high.
470 Noticeably, the discrepancy between the two quantities before
471 their convergence is wider, when N_a is higher. This is because
472 the higher N_a , the lower the achievable rate at low SNRs,

473 which is shown by comparing the solid curves. This echoes
 474 our observations of Fig. 11, namely that a higher N_a leads
 475 to a reduced separability and consequently both to a higher
 476 overall error probability and to a lower achievable rate. In
 477 fact, the achievable rate becomes especially insightful after
 478 being compared to the DCMC capacity, where we may tell
 479 how a realistic decoupled detection performs and how far its
 480 performance is from the DCMC capacity.

481 V. CONCLUSION

482 In this paper, we introduced the concept of our GPSM
 483 scheme and carried out its theoretical analysis in terms of both
 484 its DCMC capacity as well as its achievable rate relying on our
 485 analytical upper bound of the SER and the BER expressions,
 486 when a low-complexity decoupled detector is employed. Our
 487 numerical results demonstrate that the upper bound introduced
 488 is tight and the DCMC capacity analysis indicates that our
 489 GPSM scheme constitutes a flexible MIMO arrangement. Our
 490 future work will consider a range of other low-complexity
 491 MIMO schemes, such as the receive antenna selection and the
 492 classic SM, in the context of large-scale MIMOs.

493 Furthermore, the insights of our error probability and capac-
 494 ity analysis are multi-folds:

- 495 • It can be seen that there is a gap between the DCMC
 496 capacity relying on ML detection and the achievable rate
 497 of decoupled detection. Thus, a novel detection method is
 498 desired for closing this gap and for striking a better trade-
 499 off between the performance attained and the complexity
 500 imposed.
- 501 • The error probability derived serves as a tight upper bound
 502 of our GPSM performance. This facilitates the convenient
 503 study of finding beneficial bit-to-symbol mapping and
 504 error-probability balancing between the spatial symbols
 505 and conventional modulated symbols [25]. Otherwise,
 506 excessive-complexity bit-by-bit Monte-Carlo simulations
 507 would be required.
- 508 • Furthermore, both the capacity and error probability anal-
 509 ysis provide a bench-marker for conducting further re-
 510 search on antenna selection techniques for our GPSM
 511 scheme, where different criteria may be adopted either
 512 for maximizing the capacity or for minimizing the error
 513 probability, again without excessive-complexity bit-by-bit
 514 Monte-Carlo simulations.

515 APPENDIX A

516 PROOF OF LEMMA III.1

517 Let $\mathcal{A}_{k_{ant}}$ denote the alphabet of the spatial symbol having
 518 k_{ant} bits of information. Then the cardinality of the alphabet
 519 $\mathcal{A}_{k_{ant}}$ is twice higher compared to that of $\mathcal{A}_{k_{ant}-1}$. Thus,
 520 $\mathcal{A}_{k_{ant}}$ may be constructed by two sub-alphabets of $\mathcal{A}_{k_{ant}-1}$,
 521 represented by 0 and 1, respectively. We may thereafter refer to
 522 the alphabet of $\mathcal{A}_{k_{ant}-1}$ preceded by the above-mentioned with
 523 0 (1) as zero-alphabet (one-alphabet).

524 Assuming that the spatial symbol representing k_{ant} zeros
 525 was transmitted, we may then calculate the total number of
 526 pair-wise bit errors ϵ_0 in the above zero-alphabet. Hence, the

number of pair-wise bit errors ϵ_1 in the one-alphabet is simply
 $\epsilon_1 = \epsilon_0 + A$, where $A = 2^{k_{ant}}$ accounts for the difference in
 the first preceding bit. Hence the total number of pair-wise
 bit errors is $\epsilon = 2\epsilon_0 + 2^{k_{ant}}$. Taking into account an equal
 probability of $1/(2^{k_{ant}} - 1)$ for each possible spatial symbol
 error, we arrive at the correction factor given by $\delta_{k_{ant}} = (2\epsilon_0 + 2^{k_{ant}})/(2^{k_{ant}} - 1)$.

Since ϵ_0 represents the total number of pair-wise bit errors
 corresponding to case of $(k_{ant} - 1)$ bits of information, we
 have $\epsilon_0 = (2^{k_{ant}-1} - 1)\delta_{k_{ant}-1}$. Hence the resultant expres-
 sion of the correction factor may be calculated recursively
 according to (23) after some further manipulations.³

APPENDIX B

PROOF OF LEMMA III.2

Considering a general case of N_r as well as N_a and assuming
 that the RA pattern $\mathcal{C}(k)$ was activated, after substituting (3)
 into (6), we have:

$$y_{v_i} = \sqrt{\beta/N_a} b_{m_i} + w_{v_i}, \quad \forall v_i \in \mathcal{C}(k), \quad (38)$$

$$y_{u_i} = w_{u_i}, \quad \forall u_i \in \bar{\mathcal{C}}(k), \quad (39)$$

where $\bar{\mathcal{C}}(k)$ denotes the complementary set of the activated RA
 pattern $\mathcal{C}(k)$ in \mathcal{C} . Furthermore, upon introducing $\sigma_0^2 = \sigma^2/2$,
 we have:

$$|y_{v_i}|^2 = \mathcal{R}(y_{v_i})^2 + \mathcal{I}(y_{v_i})^2 \quad (40)$$

$$\sim \mathcal{N}\left(\sqrt{\beta/N_a} \mathcal{R}(b_{m_i}), \sigma_0^2\right) + \mathcal{N}\left(\sqrt{\beta/N_a} \mathcal{I}(b_{m_i}), \sigma_0^2\right), \quad (41)$$

$$|y_{u_i}|^2 = \mathcal{R}(w_{u_i})^2 + \mathcal{I}(w_{u_i})^2 \quad (42)$$

$$\sim \mathcal{N}(0, \sigma_0^2) + \mathcal{N}(0, \sigma_0^2), \quad (43)$$

where $\mathcal{R}(\cdot)$ and $\mathcal{I}(\cdot)$ represent the real and imaginary operators,
 respectively. As a result, by normalisation with respect to σ_0^2 ,
 we have the following observations:

$$|y_{v_i}|^2 \sim \chi_2^2(g; \lambda_{v_i}), \quad \forall v_i \in \mathcal{C}(k), \quad (44)$$

$$|y_{u_i}|^2 \sim \chi_2^2(g), \quad \forall u_i \in \bar{\mathcal{C}}(k), \quad (45)$$

where the non-centrality is given by $\lambda_{v_i} = \beta|b_{m_i}|^2/N_a\sigma_0^2$.
 Exploiting the fact that $\mathbb{E}[|b_{m_i}|^2] = 1$, $\forall i$ (or $|b_{m_i}|^2 = 1$, $\forall i$ for
 PSK modulation), we have $\lambda = \lambda_{v_i}$, $\forall v_i$. Note that λ is also a
 random variable obeying the distribution of $f_\lambda(\lambda)$.

Recall from (8) that the correct decision concerning the
 spatial symbols occurs, when $\sum_{i=1}^{N_a} |y_{v_i}|^2$ is the maximum.
 By exploiting the fact that $\mathbb{E}_{\mathcal{C}(k)}[\Delta] = \Delta$, the correct detection
 probability Δ of the spatial symbols given the non-centrality λ ,

³By assuming equal-probability erroneously detected patterns, a spatial
 symbol may be mistakenly detected as any of the other spatial symbols with
 equal probability. Let us now give an example for highlighting the rationale
 of introducing the correction factor. For example, spatial symbol '0' carrying
 bits [0,0] was transmitted, it would result into a one-bit difference when the
 spatial symbol '1' carrying [0,1] or '2' carrying [1,0] was erroneously detected.
 However, it would result into a two-bits difference when spatial symbol '3'
 carrying [1,1] was erroneously detected. This corresponds to four bit errors
 in total for these three cases, thus a correction factor of 4/3 is needed when
 converting the symbol error ratio to bit error ratio.

when the RA pattern $\mathcal{C}(k)$ was activated may be lower bounded as in (46). (See equation at bottom of page) More explicitly,

- equation (a) serves as the lower bound, since it sets the most strict condition for the correct detection, when each metric y_{u_j} of the inactivated RA indices in $\bar{\mathcal{C}}(k)$ is lower than each metric g_{v_i} of the activated RA indices in $\mathcal{C}(k)$. Note that, equality holds when $N_a = 1$;
- equation (b) follows from the fact that the N_a random variables $|y_{v_i}|^2$ are independent of each other;
- equation (c) follows from the fact that the $(N_r - N_a)$ random variables $|y_{u_j}|^2$ are independent and equation (d) follows from the fact that the N_a independent variables of $|y_{v_i}|^2$ and the $(N_r - N_a)$ independent variables of $|y_{u_j}|^2$ are both identically distributed.

As a result, after averaging over the distribution of $f_\lambda(\lambda)$, the analytical SER e_{ant}^s of the spatial symbol in our GPSM scheme may be upper bounded as in (25). In general, the expression of $f_\lambda(\lambda)$ can be acquired with the aid of the empirical histogram based method, while in case the loose/stringent power-normalisation factor of (4)/(5) is used, the analytical expression for $f_\lambda(\lambda)$ is given in Lemma III.3/Lemma III.4.

APPENDIX C

PROOF OF LEMMA III.3

Upon expanding the expression of λ in (26) by taking into account (4), we have:

$$\lambda = \frac{\beta_l}{N_a \sigma_0^2} = \frac{N_r}{N_a \sigma_0^2 \text{Tr}[(\mathbf{H}\mathbf{H}^H)^{-1}]}. \quad (47)$$

Consider first the distribution of $\text{Tr}[(\mathbf{H}\mathbf{H}^H)^{-1}]$ and let $\mathbf{W} = \mathbf{H}\mathbf{H}^H$. Since the entries of \mathbf{H} are i.i.d. zero-mean unit-

variance complex Gaussian random variables, \mathbf{W} obeys a complex Wishart distribution. Hence the joint PDF of its eigenvalues $\{\lambda_{\mathbf{W}_i}\}_{i=1}^{N_r}$ is given by [26], [27]

$$f_{\mathbf{W}}(\{\lambda_{\mathbf{W}_i}\}_{i=1}^{N_r}) = \frac{K^{-1}}{N_r!} \prod_i e^{-\lambda_{\mathbf{W}_i}} \lambda_{\mathbf{W}_i}^{N_t - N_r} \prod_{i < j} (\lambda_{\mathbf{W}_i} - \lambda_{\mathbf{W}_j})^2, \quad (48)$$

where K is a normalising factor. Thus for its inverse $\mathbf{U} = \mathbf{W}^{-1}$, we have

$$f_{\mathbf{U}}(\{\lambda_{\mathbf{U}_i}\}_{i=1}^{N_r}) = \prod_i \lambda_{\mathbf{U}_i}^{-2} f_{\mathbf{W}}(\{\lambda_{\mathbf{W}_i}^{-1}\}_{i=1}^{N_r}). \quad (49)$$

Furthermore, since $\text{Tr}[\mathbf{U}] = \sum \lambda_{\mathbf{U}_i}$, where $\{\lambda_{\mathbf{U}_i}\}_{i=1}^{N_r}$ is the eigenvalues of \mathbf{U} , we have the CDF of $\text{Tr}[\mathbf{U}]$ given by (50), where $T_1 = T$ and $t_1 = 1/T$, while $\forall j > 1$

$$T_j = T - \sum_{i=1}^{j-1} \lambda_{\mathbf{U}_i}, \quad \frac{t_j - 1}{\left(T - \sum_{i=1}^{j-1} \lambda_{\mathbf{U}_i}^{-1}\right)}.$$

Let $\lambda_0 = 1/\text{Tr}[\mathbf{U}]$. Then, from the above analysis we know that the PDF of $f_{\text{Tr}[\mathbf{U}]}$ is the derivative of (50). (See equation at the bottom of the page) Hence, we may also get the PDF of $f_{\lambda_0}(\lambda_0) = \lambda_0^{-2} f_{\text{Tr}[\mathbf{U}]}(\lambda_0^{-1})$. Finally, since $\lambda_0 = \lambda N_a \sigma_0^2 / N_r$, we have $f_\lambda(\lambda) = N_a \sigma_0^2 f_{\lambda_0}(\lambda N_a \sigma_0^2 / N_r) / N_r$. After simple manipulations, we have (27).

APPENDIX D

PROOF OF LEMMA III.4

Upon expanding the expression of λ in (26) by taking into account (5), we have:

$$\lambda = \frac{\beta_s}{N_a \sigma_0^2} = \frac{1}{\sigma_0^2 \mathbf{s}^H (\mathbf{H}\mathbf{H}^H)^{-1} \mathbf{s}}. \quad (51)$$

$$\begin{aligned} \Delta &\stackrel{a}{\geq} \int_0^\infty P(|y_{u_1}|^2 < g_{v_1}, \dots, |y_{u_{N_r - N_a}}|^2 < g_{v_1}, \dots, |y_{u_1}|^2 < g_{v_{N_a}}, \dots, |y_{u_{N_r - N_a}}|^2 < g_{v_{N_a}}) \\ &\quad \cdot P(|y_{v_1}|^2 = g_{v_1}, \dots, |y_{v_{N_a}}|^2 = g_{v_{N_a}} | \lambda_{v_1}, \dots, \lambda_{v_{N_a}}) dg_{v_1} \cdots dg_{v_{N_a}} \\ &\stackrel{b}{=} \prod_{i=1}^{N_a} \int_0^\infty P(|y_{u_1}|^2 < g_{v_i}, \dots, |y_{u_{N_r - N_a}}|^2 < g_{v_i}) P(|y_{v_i}|^2 = g_{v_i} | \lambda_{v_i}) dg_{v_i} \\ &\stackrel{c}{=} \prod_{i=1}^{N_a} \int_0^\infty \prod_{u_j \in \bar{\mathcal{C}}(k)} P(|y_{u_j}|^2 < g_{v_i}) P(|y_{v_i}|^2 = g_{v_i} | \lambda_{v_i}) dg_{v_i} \\ &\stackrel{d}{=} \left\{ \int_0^\infty [F_{\chi^2_2}(g)]^{N_r - N_a} f_{\chi^2_2}(g; \lambda) dg \right\}^{N_a} \end{aligned} \quad (46)$$

$$F_{\text{Tr}[\mathbf{U}]}(T) = \int_0^{T_1} \int_0^{T_2} \cdots \int_0^{T_{N_r}} f_{\mathbf{U}}(\{\lambda_{\mathbf{U}_i}\}_{i=1}^{N_r}) d\lambda_{\mathbf{U}_{N_r}} \cdots d\lambda_{\mathbf{U}_1} = \int_{t_1}^\infty \int_{t_2}^\infty \cdots \int_{t_{N_r}}^\infty f_{\mathbf{W}}(\{\lambda_{\mathbf{U}_i}^{-1}\}_{i=1}^{N_r}) d\lambda_{\mathbf{U}_{N_r}}^{-1} \cdots d\lambda_{\mathbf{U}_1}^{-1} \quad (50)$$

Since the entries of \mathbf{H} are i.i.d. zero-mean unit-variance complex Gaussian random variables, $\mathbf{H}\mathbf{H}^H$ obeys a complex Wishart distribution with N_r dimensions and $2N_t$ degrees of freedom, where we have:

$$\mathbf{H}\mathbf{H}^H \sim \mathcal{CW}(\Sigma, N_r, 2N_t), \quad (52)$$

with $\Sigma = (1/2)I_{N_r}$ being the variance. By exploiting proposition 8.9 from [28] and letting $\lambda_0 = [\mathbf{s}^H(\mathbf{H}\mathbf{H}^H)^{-1}\mathbf{s}]^{-1}$, we have:

$$\lambda_0 \sim \mathcal{CW}[(\mathbf{s}^H \Sigma^{-1} \mathbf{s})^{-1}, 1, 2(N_t - N_r + 1)], \quad (53)$$

where $A \sim B$ stands for A follows the distribution of B . According to [28], the above one-dimensional complex-valued Wishart distribution is actually a chi-square distribution with $2(N_t - N_r + 1)$ degrees of freedom and scaling parameter of $(\mathbf{s}^H \Sigma^{-1} \mathbf{s})^{-1} = 1/2N_a$. Thus, the PDF of λ_0 may be explicitly written as:

$$\begin{aligned} f_{\lambda_0}(\lambda_0) &= f_{\chi^2}[2N_a\lambda_0; 2(N_t - N_r + 1)] \\ &= 2N_a \frac{e^{-\lambda_0 N_a} (2N_a \lambda_0)^{N_t - N_r}}{2^{N_t - N_r + 1} (N_t - N_r)!} \\ &= \frac{N_a^{N_t - N_r + 1} e^{-\lambda_0 N_a} \lambda_0^{N_t - N_r}}{(N_t - N_r)!}. \end{aligned} \quad (54)$$

Finally, since $\lambda_0 = \sigma_0^2 \lambda$, we have $f_\lambda(\lambda) = \sigma_0^2 f_{\lambda_0}(\sigma_0^2 \lambda)$, which is (28).

APPENDIX E

PROOF OF LEMMA III.5

The SER of \tilde{e}_{mod}^s is constituted by the SER of e_{mod}^s , when the detection of the spatial symbol is correct having a probability of $(1 - e_{\text{ant}}^s)$, plus the SER, when the detection of the spatial symbol is erroneous having a probability of e_{ant}^s , which is expressed as

$$\begin{aligned} \tilde{e}_{\text{mod}}^s &\stackrel{a}{=} (1 - e_{\text{ant}}^s) e_{\text{mod}}^s \\ &\quad + e_{\text{ant}}^s \sum_{\ell \neq k} P_{k \rightarrow \ell} \underbrace{\frac{N_c e_{\text{mod}}^s + N_d e_o^s}{N_a}}_E, \\ &\stackrel{b}{<} (1 - e_{\text{ant}}^s) e_{\text{mod}}^{s,ub} \\ &\quad + e_{\text{ant}}^s \sum_{\ell \neq k} P_{k \rightarrow \ell} \frac{N_c e_{\text{mod}}^{s,ub} + N_d e_o^s}{N_a}, \\ &\stackrel{c}{\leq} (1 - e_{\text{ant}}^s) e_{\text{mod}}^{s,ub} \\ &\quad + \frac{e_{\text{ant}}^s}{(2^{k_{\text{ant}}} - 1)} \sum_{\ell \neq k} \frac{N_c e_{\text{mod}}^{s,ub} + N_d e_o^s}{N_a}, \\ &\stackrel{d}{\leq} (1 - e_{\text{ant}}^s) e_{\text{mod}}^{s,ub} \\ &\quad + e_{\text{ant}}^s \underbrace{\sum_{\ell \neq k} \frac{N_c e_{\text{mod}}^{s,ub} + N_d e_o^s}{N_a (2^{k_{\text{ant}}} - 1)}}_A = \tilde{e}_{\text{mod}}^{s,ub}. \end{aligned}$$

Regarding the second additive term of (a), the true activated RA pattern $\mathcal{C}(k)$ may be erroneously deemed to be any of the other

legitimate RA patterns $\mathcal{C}(\ell) \in \mathcal{C}, \ell \neq k$ with a probability of $P_{k \rightarrow \ell}$, which we have to average over. As for the calculation of the per-case error rates E , when $\mathcal{C}(k)$ was erroneously detected as a particular $\mathcal{C}(\ell)$, we found that it was constituted by the error rates of e_{mod}^s for those N_c RAs in common (which maybe regarded as being partially correctly detected) and the error rates of e_o^s for those RAs that were exclusively hosted by $\mathcal{C}(\ell)$, but were excluded from $\mathcal{C}(k)$. Furthermore, since only random noise may be received by those N_d RAs in $\mathcal{C}(\ell)$, thus e_o^s simply represents the SER as a result of a random guess, i.e. we have $e_o^s = (M - 1)/M$. Let us now provide some further detailed discussions of the relations ranging from (b) to (d):

- relation (b) holds true, since \tilde{e}_{mod}^s is a monotonic function of e_{mod}^s , thus it is upper bounded upon replacing e_{mod}^s by $e_{\text{mod}}^{s,ub}$;
- although it is natural that patterns with a higher N_c would be more likely to cause an erroneous detection, we assume an equal probability of $P_{k \rightarrow \ell} = 1/(2^{k_p} - 1)$. The equal probability assumption thus puts more weight on the patterns having higher N_d , since we have $e_o^s > e_{\text{mod}}^{s,ub}$. This leads to the relation of (c). Note that, equality holds when $N_a = 1$, where $N_c = 0$ and $N_d = 1$;
- replacing e_{ant}^s by $e_{\text{ant}}^{s,ub}$ puts more weight on the second additive term of (d), since having $e_o^s > e_{\text{mod}}^{s,ub}$ leads to the relation of $A > e_{\text{mod}}^{s,ub}$. As a result (d) also holds. Again, equality holds when $N_a = 1$, where $e_{\text{ant}}^s = e_{\text{ant}}^{s,ub}$ as indicated by Lemma III.2.

ACKNOWLEDGMENT

The financial support of the EPSRC under the India-UK Advanced Technology Centre (IU-ATC), that of the EU under the Concerto project as well as that of the European Research Council's (ERC) Advance Fellow Grant is gratefully acknowledged.

REFERENCES

- R. Zhang and L. Hanzo, "Wireless cellular networks," *IEEE Veh. Technol. Mag.*, vol. 5, no. 4, pp. 31–39, Dec. 2010.
- P. Wolniansky, G. Foschini, G. Golden, and R. Valenzuela, "V-BLAST: An architecture for realizing very high data rates over the rich-scattering wireless channel," in *Proc. URSI Int. Symp. Signals, Syst., Electron.*, 1998, pp. 295–300.
- S. Alamouti, "A simple transmit diversity technique for wireless communications," *IEEE J. Sel. Areas Commun.*, vol. 16, no. 8, pp. 1451–1458, Oct. 1998.
- Q. Spencer, C. Peel, A. Swindlehurst, and M. Haardt, "An introduction to the multi-user MIMO downlink," *IEEE Commun. Mag.*, vol. 42, no. 10, pp. 60–67, Oct. 2004.
- D. Gesbert, M. Kountouris, R. Heath, C.-B. Chae, and T. Salzer, "Shifting the MIMO paradigm," *IEEE Signal Process. Mag.*, vol. 24, no. 5, pp. 36–46, Sep. 2007.
- H. Zhang and H. Dai, "Cochannel interference mitigation and cooperative processing in downlink multicell multiuser MIMO networks," *EURASIP J. Wireless Commun. Netw.*, vol. 2004, no. 2, pp. 222–235, Dec. 2004.
- R. Zhang and L. Hanzo, "Cooperative downlink multicell preprocessing relying on reduced-rate back-haul data exchange," *IEEE Trans. Veh. Technol.*, vol. 60, no. 2, pp. 539–545, Feb. 2011.
- T. Marzetta, "Noncooperative cellular wireless with unlimited numbers of base station antennas," *IEEE Trans. Wireless Commun.*, vol. 9, no. 11, pp. 3590–3600, Nov. 2010.

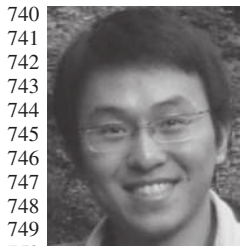
- [9] F. Rusek *et al.*, "Scaling up MIMO: Opportunities and challenges with very large arrays," *IEEE Signal Process. Mag.*, vol. 30, no. 1, pp. 40–60, Jan. 2013.
- [10] V. Cadambe and S. Jafar, "Interference alignment and degrees of freedom of the K-user interference channel," *IEEE Trans. Inf. Theory*, vol. 54, no. 8, pp. 3425–3441, Aug. 2008.
- [11] A. Molisch and M. Win, "MIMO systems with antenna selection," *IEEE Microw. Mag.*, vol. 5, no. 1, pp. 46–56, Mar. 2004.
- [12] A. Mohammadi and F. Ghannouchi, "Single RF front-end MIMO transceivers," *IEEE Commun. Mag.*, vol. 49, no. 12, pp. 104–109, Dec. 2011.
- [13] R. Mesleh, H. Haas, S. Sinanovic, C. W. Ahn, and S. Yun, "Spatial modulation," *IEEE Trans. Veh. Technol.*, vol. 57, no. 4, pp. 2228–2241, Jul. 2008.
- [14] M. Di Renzo, H. Haas, and P. M. Grant, "Spatial modulation for multiple-antenna wireless systems: A survey," *IEEE Commun. Mag.*, vol. 49, no. 12, pp. 182–191, Dec. 2011.
- [15] J. Wang, S. Jia, and J. Song, "Generalised spatial modulation system with multiple active transmit antennas and low complexity detection scheme," *IEEE Trans. Wireless Commun.*, vol. 11, no. 4, pp. 1605–1615, Apr. 2012.
- [16] L.-L. Yang, "Transmitter preprocessing aided spatial modulation for multiple-input multiple-output systems," in *Proc. IEEE 73rd VTC Spring*, 2011, pp. 1–5.
- [17] R. Zhang, L.-L. Yang, and L. Hanzo, "Generalised pre-coding aided spatial modulation," *IEEE Trans. Wireless Commun.*, vol. 12, no. 11, pp. 5434–5443, Nov. 2013.
- [18] A. Stavridis, S. Sinanovic, M. D. Renzo, and H. Haas, "Transmit precoding for receive spatial modulation using imperfect channel knowledge," in *Proc. IEEE 75th VTC Spring*, 2012, pp. 1–5.
- [19] C. Peel, B. Hochwald, and A. Swindlehurst, "A vector-perturbation technique for near-capacity multiuser communication—Part I: Channel inversion and regularization," *IEEE Trans. Commun.*, vol. 53, no. 1, pp. 195–202, Jan. 2005.
- [20] Q. Spencer, A. Swindlehurst, and M. Haardt, "Zero-forcing methods for downlink spatial multiplexing in multiuser MIMO channels," *IEEE Trans. Signal Process.*, vol. 52, no. 2, pp. 461–471, Feb. 2004.
- [21] M. Di Renzo and H. Haas, "Bit error probability of SM-MIMO over generalized fading channels," *IEEE Trans. Veh. Technol.*, vol. 61, no. 3, pp. 1124–1144, Mar. 2012.
- [22] J. A. Thomas and T. M. Cover, *Elements of Information Theory*, 2nd ed. Hoboken, NJ, USA: Wiley-Interscience, 2006.
- [23] R. Gallager, *Information Theory and Reliable Communication*. New York, NY, USA: Wiley, 1968.
- [24] M. S. John Proakis, *Digital Communications*, 5th ed. New York, NY, USA: McGraw-Hill, 2008.
- [25] M. Maleki, H. Bahrami, A. Alizadeh, and N. Tran, "On the performance of spatial modulation: Optimal constellation breakdown," *IEEE Trans. Commun.*, vol. 62, no. 1, pp. 144–157, Jan. 2014.
- [26] E. Telatar, "Capacity of multi-antenna Gaussian channels," *Eur. Trans. Telecommun.*, vol. 10, no. 6, pp. 585–595, Nov./Dec. 1999.
- [27] A. Edelman, "Eigenvalues and condition numbers of random matrices," Ph.D. dissertation, Dept. Math., MIT, Cambridge, MA, USA, 1989.
- [28] M. L. Eaton, *Multivariate Statistics: A Vector Space Approach*. Hoboken, NJ, USA: Wiley, 1983.



Lie-Liang Yang (M'98–SM'02) received the B.Eng. degree in communications engineering from Shanghai TieDao University, Shanghai, China, in 1988, and the M.Eng. and Ph.D. degrees in communications and electronics from Northern (Beijing) Jiaotong University, Beijing, China, in 1991 and 1997, respectively. From June 1997 to December 1997, he was a Visiting Scientist of the Institute of Radio Engineering and Electronics, Academy of Sciences of the Czech Republic. Since December 1997, he has been with the University of Southampton, U.K., where he is the Professor of wireless communications in the School of Electronics and Computer Science. His research has covered a wide range of topics in wireless communications, networking and signal processing. He has published over 290 research papers in journals and conference proceedings, authored/co-authored three books and also published several book chapters. The details about his publications can be found at <http://www-mobile.ecs.soton.ac.uk/lly/>. He is a Fellow of the IET, served as an associate editor to the IEEE TRANSACTIONS ON VEHICULAR TECHNOLOGY and *The Journal of Communications and Networks* (JCN), and is currently an associate editor to the *IEEE Access* and the *Security and Communication Networks (SCN) Journal*.



Lajos Hanzo received the B.S. degree in electronics in 1976 and the Ph.D. degree in 1983. In 2009, he was awarded the honorary doctorate "Doctor Honoris Causa" by the Technical University of Budapest. During his 38-year career in telecommunications he has held various research and academic posts in Hungary, Germany, and the U.K. Since 1986, he has been with the School of Electronics and Computer Science, University of Southampton, U.K., where he holds the Chair in telecommunications. He has successfully supervised 80+ PhD students, co-authored 20 John Wiley/IEEE Press books on mobile radio communications totalling in excess of 10 000 pages, published 1400+ research entries at IEEE Xplore, acted both as TPC and General Chair of IEEE conferences, presented keynote lectures, and has been awarded a number of distinctions. Currently, he is directing a 100-strong academic research team working on a range of research projects in the field of wireless multimedia communications sponsored by industry, the Engineering and Physical Sciences Research Council (EPSRC) U.K., the European Research Council's Advanced Fellow Grant, and the Royal Society's Wolfson Research Merit Award. He is an enthusiastic supporter of industrial and academic liaison and he offers a range of industrial courses. He is also a Governor of the IEEE VTS. During 2008–2012, he was the Editor-in-Chief of the IEEE Press and a Chaired Professor also at Tsinghua University, Beijing. His research is funded by the European Research Council's Senior Research Fellow Grant. He has over 20 000 citations. For further information on research in progress and associated publications please refer to <http://www-mobile.ecs.soton.ac.uk>



Rong Zhang (M'09) received the B.Sc. degree from Southeast University, China, in 2003 and the Ph.D. degree from Southampton University, U.K., in 2009. Before receiving the doctorate degree, he was an Engineer from August 2003 to July 2004 at China Telecom and a Research Assistant from January 2006 to May 2009 at Mobile Virtual Center of Excellence (MVCE), U.K. After being a post-doctoral Researcher from August 2009 to July 2012 at Southampton University, he took an industrial consulting leave from August 2012 to January 2013 for

Huawei Sweden R&D, as a System Algorithms Specialist. He was appointed as a Lecturer with the CSPC Group, ECS, Southampton University, in February 2013. He has over 30 journals in prestigious publication avenues such as IEEE and OSA and many more in major conference proceedings. He regularly serves as a Reviewer for IEEE transactions/journals and has several times served as a TPC member/Invited Session Chair of major conferences. He is the recipient of joint funding from MVCE and EPSRC and is also a Visiting Researcher under Worldwide University Network (WUN). More details can be found at <http://www.ecs.soton.ac.uk/people/rz>

AUTHOR QUERIES

AUTHOR PLEASE ANSWER ALL QUERIES

AQ1 = Please be informed that the capital letters were removed from the terms “multiple input multiple output,” “generalised pre-coded aided spatial modulation,” “symbol error ratio,” “bit error ratio,” “discrete-input continuous-output memoryless channel,” and “signal to noise ratio” in the Abstract per IEEE style and also in other occurrences of these terms in lines 88 to 91 and 305 for the sake of consistency. Please check if it is correct.

AQ2 = Please provide keywords.

AQ3 = Please check changes made in first footnote and the addition of an Acknowledgment Section.

AQ4 = Please check if “30 journals” should be “30 papers” instead.

END OF ALL QUERIES

IEEE
Proof

Error Probability and Capacity Analysis of Generalised Pre-Coding Aided Spatial Modulation

Rong Zhang, *Member, IEEE*, Lie-Liang Yang, *Senior Member, IEEE*, and Lajos Hanzo

Abstract—The recently proposed multiple input multiple output (MIMO) transmission scheme termed as generalized pre-coding aided spatial modulation (GPSM) is analyzed, where the key idea is that a particular subset of receive antennas is activated and the specific activation pattern itself conveys useful implicit information. We provide the upper bound of both the symbol error ratio (SER) and bit error ratio (BER) expression of the GPSM scheme of a low-complexity decoupled detector. Furthermore, the corresponding discrete-input continuous-output memoryless channel (DCMC) capacity as well as the achievable rate is quantified. Our analytical SER and BER upper bound expressions are confirmed to be tight by our numerical results. We also show that our GPSM scheme constitutes a flexible MIMO arrangement and there is always a beneficial configuration for our GPSM scheme that offers the same bandwidth efficiency as that of its conventional MIMO counterpart at a lower signal to noise ratio (SNR) per bit.

Index Terms—Author, please supply index terms/keywords for your paper. To download the IEEE Taxonomy go to http://www.ieee.org/documents/taxonomy_v101.pdf.

I. INTRODUCTION

MULTIPLE INPUT MULTIPLE OUTPUT (MIMO) systems constitute one of the most promising recent technical advances in wireless communications, since they facilitate high-throughput transmissions in the context of various standards [1]. Hence, they attracted substantial research interests, leading to the Vertical-Bell Laboratories Layered Space-Time (V-BLAST) scheme [2] and to the classic Space Time Block Coding (STBC) arrangement [3]. The point-to-point single-user MIMO systems are capable of offering diverse transmission functionalities in terms of multiplexing-diversity and beam-forming gains. Similarly, Spatial Division Multiple Access (SDMA) employed in the uplink and multi-user MIMO techniques invoked in the downlink also constitute beneficial building blocks [4], [5]. The basic benefits of MIMOs have also been recently exploited in the context of the network MIMO

concept [6], [7], for constructing large-scale MIMOs [8], [9] and for conceiving beneficial arrangements for interference-limited MIMO scenarios [10].

Despite having a plethora of studies on classic MIMO systems, their practical constraints, such as their I/Q imbalance, their transmitter and receiver complexity as well as the cost of their multiple Radio Frequency (RF) Power Amplifier (PA) chains as well as their Digital-Analogue/Analogue-Digital (DA/AD) converters have received limited attention. To circumvent these problems, low complexity alternatives to conventional MIMO transmission schemes have also been proposed, such as the Antenna Selection (AS) [11], [12] and the Spatial Modulation (SM) [13], [14] philosophies. More specifically, SM and generalised SM [15] constitute novel MIMO techniques, which were conceived for providing a higher throughput than a single-antenna aided system, while maintaining both a lower complexity and a lower cost than the conventional MIMOs, since they may rely on a reduced number of RF up-conversion chains. To elaborate a little further, SM conveys extra information by mapping $\log_2(N_t)$ bits to the Transmit Antenna (TA) indices of the N_t TAs, in addition to the classic modulation schemes, as detailed in [13].

By contrast, the family of Pre-coding aided Spatial Modulation (PSM) schemes is capable of conveying extra information by appropriately selecting the Receive Antenna (RA) indices, as detailed in [16]. More explicitly, in PSM the indices of the RA represent additional information in the spatial domain. As a specific counterpart of the original SM, PSM benefits from both a low cost and a low complexity at the receiver side, therefore it may be considered to be eminently suitable for downlink transmissions [16]. The further improved concept of Generalised PSM (GPSM) was proposed in [17], where comprehensive performance comparisons were carried out between the GPSM scheme as well as the conventional MIMO scheme and the associated detection complexity issues were discussed. Furthermore, a range of practical issues were investigated, namely the detrimental effects of realistic imperfect Channel State Information at the Transmitter (CSIT), followed by a low-rank approximation invoked for large-dimensional MIMOs. Finally, the main difference between our GPSM scheme and the classic SM is that the former requires downlink pre-processing and CSIT, although they may be considered as a dual counterpart of each other and may hence be used in a hybrid manner. Other efforts on robust PSM was reported in [18].

Manuscript received March 17, 2014; revised June 2, 2014; accepted August 7, 2014. This work was supported by the EPSRC under the India-UK Advanced Technology Centre (IU-ATC), by the EU under the Concerto project, and by the European Research Council's (ERC) Advanced Fellow Grant. The associate editor coordinating the review of this paper and approving it for publication was M. Ardakani.

The authors are with the Communications, Signal Processing and Control, School of Electronics and Computer Science (ECS), University of Southampton, Southampton SO17 1BJ, U.K. (e-mail: rz@ecs.soton.ac.uk; lly@ecs.soton.ac.uk; lh@ecs.soton.ac.uk, <http://www-mobile.ecs.soton.ac.uk>).

Color versions of one or more of the figures in this paper are available online at <http://ieeexplore.ieee.org>.

Digital Object Identifier 10.1109/TWC.2014.2347297

As a further development, in this paper, we provide the theoretical analysis of the recently proposed GPSM scheme [17], which is not available in the literature. More explicitly, both the discrete-input continuous-output memoryless channel (DCMC) capacity as well as the achievable rate are characterized. Importantly, tight upper bounds of the symbol error ratio (SER) and bit error ratio (BER) expressions are derived, when a decoupled low-complexity detector is employed.

The rest of our paper is organised as follows. In Section II, we introduce the underlying concept as well as the detection methods of the GPSM scheme. This is followed by our analytical study in Section III, where both the DCMC capacity and the achievable rate as well as the SER/BER expressions are derived. Our simulation results are provided in Section IV, while we conclude in Section V.

II. SYSTEM MODEL

A. Conceptual Description

Consider a MIMO system equipped with N_t TAs and N_r RAs, where we assume $N_t \geq N_r$. In this MIMO set-up, a maximum of N_r parallel data streams may be supported, conveying a total of $k_{eff} = N_r k_{mod}$ bits altogether, where $k_{mod} = \log_2(M)$ denotes the number of bits per symbol of a conventional M -ary PSK/QAM scheme and its alphabet is denoted by \mathcal{A} . Transmitter Pre-Coding (TPC) relying on the TPC matrix of $\mathbf{P} \in \mathbb{C}^{N_t \times N_r}$ may be used for pre-processing the source signal before its transmission upon exploiting the knowledge of the CSIT.

In contrast to the above-mentioned classic multiplexing of N_r data streams, in our GPSM scheme a total of $N_a < N_r$ RAs are activated so as to facilitate the simultaneous transmission of N_a data streams, where the particular pattern of the N_a RAs activated conveys extra information in form of so-called spatial symbols in addition to the information carried by the conventional modulated symbols. Hence, the number of bits in GPSM conveyed by a spatial symbol becomes $k_{ant} = \lfloor \log_2(|\mathcal{C}_t|) \rfloor$, where the set \mathcal{C}_t contains all the combinations associated with choosing N_a activated RAs out of N_r RAs. As a result, the total number of bits transmitted by the GPSM scheme is $k_{eff} = k_{ant} + N_a k_{mod}$. Finally, it is plausible that the conventional MIMO scheme obeys $N_a = N_r$. For assisting further discussions, we also let $\mathcal{C}(k)$ and $\mathcal{C}(k, i)$ denote the k th RA activation pattern and the i th activated RA in the k th activation pattern, respectively.

B. GPSM Transmitter

More specifically, let \mathbf{s}_m^k be an explicit representation of a so-called super-symbol $\mathbf{s} \in \mathbb{C}^{N_r \times 1}$, indicating that the RA pattern k is activated and N_a conventional modulated symbols $\mathbf{b}_m = [b_{m1}, \dots, b_{mN_a}]^T \in \mathbb{C}^{N_a \times 1}$ are transmitted, where we have $b_{m_i} \in \mathcal{A}$ and $\mathbb{E}[|b_{m_i}|^2] = 1$, $\forall i \in [1, N_a]$. In other words, we have the relationship

$$\mathbf{s}_m^k = \mathbf{\Omega}_k \mathbf{b}_m, \quad (1)$$

where $\mathbf{\Omega}_k = \mathbf{I}[:, \mathcal{C}(k)]$ is constituted by the specifically selected columns determined by $\mathcal{C}(k)$ of an identity matrix of \mathbf{I}_{N_r} . Following TPC, the resultant transmit signal $\mathbf{x} \in \mathbb{C}^{N_t \times 1}$ may be written as

$$\mathbf{x} = \sqrt{\beta/N_a} \mathbf{P} \mathbf{s}_m^k. \quad (2)$$

To avoid dramatic power fluctuation during the pre-processing, we introduce the scaling factor of β designed for maintaining either the loose power-constraint of $\mathbb{E}[\|\mathbf{x}\|^2] = 1$ or the strict power-constraint of $\|\mathbf{x}\|^2 = 1$, which are thus denoted by β_l and β_s , respectively.

As a natural design, the TPC matrix has to ensure that no energy leaks into the unintended RA patterns. Hence, the classic linear Channel Inversion (CI)-based TPC [19], [20] may be used, which is formulated as

$$\mathbf{P} = \mathbf{H}^H (\mathbf{H} \mathbf{H}^H)^{-1} \quad (3)$$

where the power-normalisation factor of the output power after pre-processing is given by

$$\beta_l = \frac{N_r}{\text{Tr}[(\mathbf{H} \mathbf{H}^H)^{-1}]}, \quad (4)$$

$$\beta_s = \frac{N_a}{\mathbf{s}^H (\mathbf{H} \mathbf{H}^H)^{-1} \mathbf{s}}. \quad (5)$$

The stringent power-constraint of (5) is less common than the loose power-constraint of (4). The former prevents any of the power fluctuations at the transmitter, which was also considered in [19]. For completeness, we include both power-constraints in this paper.

C. GPSM Receiver

The signal observed at the N_r RAs may be written as

$$\mathbf{y} = \sqrt{\beta/N_a} \mathbf{H} \mathbf{P} \mathbf{s}_m^k + \mathbf{w}, \quad (6)$$

where $\mathbf{w} \in \mathbb{C}^{N_r \times 1}$ is the circularly symmetric complex Gaussian noise vector with each entry having a zero mean and a variance of σ^2 , i.e. we have $\mathbb{E}[\|\mathbf{w}\|^2] = \sigma^2 \mathbf{I}_{N_r}$, while $\mathbf{H} \in \mathbb{C}^{N_r \times N_t}$ represents the MIMO channel involved. We assume furthermore that each entry of \mathbf{H} undergoes frequency-flat Rayleigh fading and it is uncorrelated between different super-symbol transmissions, while remains constant within the duration of a super-symbol's transmission. The super-symbols transmitted are statistically independent from the noise.

At the receiver, the joint detection of both the conventional modulated symbols \mathbf{b}_m and of the spatial symbol k obeys the Maximum Likelihood (ML) criterion, which is formulated as

$$[\hat{m}_1, \dots, \hat{m}_{N_a}, \hat{k}] = \arg \min_{\mathbf{s}_n^\ell \in \mathcal{B}} \left\{ \left\| \mathbf{y} - \sqrt{\beta/N_a} \mathbf{H} \mathbf{P} \mathbf{s}_n^\ell \right\|^2 \right\}, \quad (7)$$

where $\mathcal{B} = \mathcal{C} \times \mathcal{A}^{N_a}$ is the joint search space of the super-symbol \mathbf{s}_n^ℓ . Alternatively, decoupled or separate detection may also be employed, which treats the detection of the conventional

172 modulated symbols \mathbf{b}_m and the spatial symbol k separately. In
173 this reduced-complexity variant,¹ we have

$$\begin{aligned}\hat{k} &= \arg \max_{\ell \in [1, |\mathcal{C}|]} \left\{ \sum_{i=1}^{N_a} |y_{\mathcal{C}(\ell, i)}|^2 \right\}, \\ \hat{m}_i &= \arg \min_{n_i \in [1, M]} \left\{ \left| y_{\hat{v}_i} - \sqrt{\beta/N_a} \mathbf{h}_{\hat{v}_i} \mathbf{p}_{\hat{v}_i} b_{n_i} \right|^2 \right\}_{\hat{v}_i = \mathcal{C}(\hat{k}, i)},\end{aligned}\quad (8)$$

174 where $\mathbf{h}_{\hat{v}_i}$ is the \hat{v}_i th row of \mathbf{H} representing the channel
175 between the \hat{v}_i th RA and the transmitter, while $\mathbf{p}_{\hat{v}_i}$ is the \hat{v}_i th
176 column of \mathbf{P} representing the \hat{v}_i th TPC vector. Thus, correct
177 detection is declared, when we have $\hat{k} = k$ and $\hat{m}_i = m_i$, $\forall i$.

178 *Remarks:* Note that the complexity of the ML detection of
179 (7) is quite high, which is on the order determined by the
180 super-alphabet \mathcal{B} , hence obeying $\mathcal{O}(|\mathcal{C}|M^{N_a})$. By contrast, the
181 decoupled detection of (8) and (9) facilitates a substantially
182 reduced complexity compared to that of (7). More explicitly, the
183 complexity is imposed by detecting N_a conventional modulated
184 symbols, plus the complexity (κ) imposed by the comparisons
185 invoked for non-coherently detecting the spatial symbol of (8),
186 which may be written as $\mathcal{O}(N_a M + \kappa)$. Further discussions
187 about the detection complexity of the decoupled detection of
188 the GPSM scheme may be found in [17], where the main
189 conclusion is that the complexity of the decoupled detection
190 of the GPSM scheme is no higher than that of the conventional
191 MIMO scheme corresponding to $N_a = N_r$.

192 III. PERFORMANCE ANALYSIS

193 We continue by investigating the DCMC capacity of our
194 GPSM scheme, when the joint detection scheme of (7) is
195 used and then quantify its achievable rate, when the realistic
196 decoupled detection of (8) and (9) is employed. The achievable
197 rate expression requires the theoretical BER/SER analysis of
198 the GPSM scheme, which provides more insights into the inner
199 nature of our GPSM scheme.²

200 A. DCMC Capacity and Achievable Rate

201 Both Shannon's channel capacity and its MIMO generalisa-
202 tion are maximized, when the input signal obeys a Gaussian
203 distribution [22]. Our GPSM scheme is special in the sense that
204 the spatial symbol conveys integer values constituted by the RA

¹The reduced complexity receiver operates in a decoupled manner, which is beneficial in the scenario considered, where the spatial symbols and the conventionally modulated symbols are independent. However, this assumption may not be ideal, when correlations exist between the spatial symbols and the conventionally modulated symbols. In this case, an iterative detection exchanging extrinsic soft-information between the spatial symbols and conventionally modulated symbols may be invoked. Importantly, the iterations would exploit the beneficial effects of improving the soft-information by taking channel decoding into account as well for simultaneously exploiting the underlying correlations, which is reminiscent of the detection of correlated source. A further inspiration would be to beneficially map the symbols to both the spatial and to the conventional domain at the transmitter, so that the benefits of unequal protection could be exploited.

²The Pair-wise Error Probability (PEP) analysis, relying on error events [21], was conducted in our previous contribution for the specific scenario of ML based detection [17]. In this paper, our error probability analysis is dedicated to the low-complexity decoupled detection philosophy

pattern index, which does not obey the shaping requirements of 205 Gaussian signalling. This implies that the channel capacity of 206 the GPSM scheme depends on a mixture of a continuous and 207 a discrete input. Hence, for simplicity's sake, we discuss the 208 DCMC capacity and the achievable rate of our GPSM scheme 209 in the context of discrete-input signalling for both the spatial 210 symbol and for the conventional modulated symbols mapped 211 to it. 212

1) *DCMC Capacity:* Upon recalling the received signal ob- 213 served at the N_r RAs expressed in (6), the conditional probabil- 214 ity of receiving \mathbf{y} given that a $\mathcal{M} = |\mathcal{C}|M^{N_a}$ -ary super-symbol 215 $\mathbf{s}_\tau \in \mathcal{B}$ was transmitted over Rayleigh channel and subjected to 216 the TPC of (3) is formulated as 217

$$p(\mathbf{y}|\mathbf{s}_\tau) = \frac{1}{\pi\sigma^2} \exp \left\{ -\frac{\|\mathbf{y} - \mathbf{G}\mathbf{s}_\tau\|^2}{\sigma^2} \right\}, \quad (10)$$

where $\mathbf{G} = \sqrt{\beta/N_a} \mathbf{H} \mathbf{P}$. The DCMC capacity of the ML- 218 based joint detection of our GPSM scheme is given by [23] 219

$$C = \max_{p(\mathbf{s}_1), \dots, p(\mathbf{s}_M)} \sum_{\tau=1}^M \int_{-\infty}^{\infty} p(\mathbf{y}, \mathbf{s}_\tau) \log_2 \left(\frac{p(\mathbf{y}|\mathbf{s}_\tau)}{\sum_{\epsilon=1}^M p(\mathbf{y}, \mathbf{s}_\epsilon)} \right) d\mathbf{y}, \quad (11)$$

which is maximized, when we have $p(\mathbf{s}_\tau) = 1/M$, $\forall \tau$ [23]. 220 Furthermore, we have 221

$$\begin{aligned}\log_2 \left(\frac{p(\mathbf{y}|\mathbf{s}_\tau)}{\sum_{\epsilon=1}^M p(\mathbf{y}, \mathbf{s}_\epsilon)} \right) &= \log_2 \left(\frac{p(\mathbf{y}|\mathbf{s}_\tau)}{\sum_{\epsilon=1}^M p(\mathbf{y}|\mathbf{s}_\epsilon) p(\mathbf{s}_\epsilon)} \right) \\ &= -\log_2 \left(\frac{1}{M} \sum_{\epsilon=1}^M \frac{p(\mathbf{y}|\mathbf{s}_\epsilon)}{p(\mathbf{y}|\mathbf{s}_\tau)} \right) \\ &= \log_2(M) - \log_2 \sum_{\epsilon=1}^M \exp(\Psi),\end{aligned}\quad (12)$$

where substituting (10) into (12), the term Ψ is expressed as 222

$$\Psi = \frac{-\|\mathbf{G}(\mathbf{s}_\tau - \mathbf{s}_\epsilon) + \mathbf{w}\|^2 + \|\mathbf{w}\|^2}{\sigma^2}. \quad (13)$$

Finally, by substituting (12) into (11) and exploiting that $p(\mathbf{s}_\tau) = 223$ $1/M$, $\forall \tau$, we have 224

$$C = \log_2(M) - \frac{1}{M} \sum_{\tau=1}^M \mathbb{E}_{\mathbf{G}, \mathbf{w}} \left[\log_2 \sum_{\epsilon=1}^M \exp(\Psi) \right]. \quad (14)$$

2) *Achievable Rate:* The above DCMC capacity expression 225 implicitly relies on the ML-based joint detection of (7), which 226 has a complexity on the order of $\mathcal{O}(M)$. When the reduced- 227 complexity decoupled detection of (8) and (9) is employed, we 228 estimate the achievable rate based on the mutual information 229 $I(z; \hat{z})$ per bit measured for our GPSM scheme between the 230 input bits $z \in [0, 1]$ and the corresponding demodulated output 231 bits $\hat{z} \in [0, 1]$. 232

The mutual information per bit $I(z; \hat{z})$ is given for the Binary 233 Symmetric Channel (BSC) by [22]: 234

$$I(z; \hat{z}) = H(z) - H(z|\hat{z}), \quad (15)$$

where $H(z) = -\sum_z P_z \log_2 P_z$ represents the entropy of the input bits z and P_z is the Probability Mass Function (PMF) of z . It is noted furthermore that we have $H(z) = 1$, when we adopt the common assumption of equal-probability bits, i.e. $P_{z=0} = P_{z=1} = 1/2$. On the other hand, the conditional entropy $H(z|\hat{z})$ represents the average uncertainty about z after observing \hat{z} , which is given by:

$$H(z|\hat{z}) = \sum_{\hat{z}} P_{\hat{z}} \left[\sum_z P_{z|\hat{z}} \log_2 P_{z|\hat{z}} \right] = -e_x \log_2 e_x - (1 - e_x) \log_2 (1 - e_x), \quad (16)$$

where e_x is the crossover probability. By substituting (16) into (15) and exploiting $H(z) = 1$ we have:

$$I(z; \hat{z}) = 1 + e_x \log_2 e_x + (1 - e_x) \log_2 (1 - e_x). \quad (17)$$

Since the input bit in our GPSM scheme may be mapped either to a spatial symbol or to a conventional modulated symbol with a probability of k_{ant}/k_{eff} and $N_a k_{mod}/k_{eff}$, respectively, the achievable rate becomes

$$R = k_{ant} I(e_x = e_{ant}^b) + N_a k_{mod} I(e_x = \tilde{e}_{mod}^b), \quad (18)$$

where e_{ant}^b represents the BER of the spatial symbol, while \tilde{e}_{mod}^b represents the BER of the conventional modulated symbols in the presence of spatial symbol errors due to the detection of (8).

B. Error Probability

1) *The Expression of e_{eff}^s and e_{eff}^b* : Let us first let e_{ant}^s represent the SER of the spatial symbol, while \tilde{e}_{mod}^s represent the SER of the conventional modulated symbols in the presence of spatial symbol errors. Let further N_{ant}^e and N_{mod}^e represent the number of symbol errors in the spatial symbols and in the conventional modulated symbols, respectively. Then we have $e_{ant}^s = N_{ant}^e/N_s$ and $\tilde{e}_{mod}^s = N_{mod}^e/N_a N_s$, where N_s is the total number of GPSM symbols. Hence, the average SER e_{eff}^s of our GPSM scheme is given by:

$$e_{eff}^s = \frac{(N_{ant}^e + N_{mod}^e)}{(1 + N_a)N_s} = \frac{(e_{ant}^s + N_a \tilde{e}_{mod}^s)}{(1 + N_a)}. \quad (19)$$

Similarly, the average BER e_{eff}^b of our GPSM scheme may be written as:

$$e_{eff}^b = \frac{(k_{ant} e_{ant}^b + N_a k_{mod} \tilde{e}_{mod}^b)}{k_{eff}} \approx \frac{(\delta_{ant} e_{ant}^s + N_a \tilde{e}_{mod}^s)}{k_{eff}}. \quad (20)$$

where the second equation of (20) follows from the relation

$$\tilde{e}_{mod}^b \approx \frac{\tilde{e}_{mod}^s}{k_{mod}}, \quad (21)$$

$$e_{ant}^b \approx \frac{\delta_{ant} e_{ant}^s}{k_{ant}}. \quad (22)$$

Importantly, we have Lemma III.1 for the expression of $\delta_{k_{ant}}$ acting as a correction factor in (22).

Lemma III.1. (Proof in Appendix A): The generic expression of the correction factor $\delta_{k_{ant}}$ for k_{ant} bits of information is given by:

$$\delta_{k_{ant}} = \delta_{k_{ant}-1} + \frac{2^{k_{ant}-1} - \delta_{k_{ant}-1}}{2^{k_{ant}} - 1}, \quad (23)$$

where given $\delta_0 = 0$, we can recursively determine $\delta_{k_{ant}}$.

Furthermore, by considering (21) and (22), the achievable rate expressed in (18) may be written as

$$R \approx k_{ant} I\left(\frac{\delta_{k_{ant}} e_{ant}^s}{k_{ant}}\right) + N_a k_{mod} I\left(\frac{\tilde{e}_{mod}^s}{k_{mod}}\right). \quad (24)$$

Hence, as suggested by (19), (20) and (24), we find that both the average error probability as well as the achievable rate of our GPSM scheme requires the entries of e_{ant}^s and \tilde{e}_{mod}^s , which will be discussed as follows.

2) *Upper Bound of e_{ant}^s* : We commence our discussion by directly formulating the following lemma:

Lemma III.2. (Proof in Appendix B): The upper bound of the analytical SER of the spatial symbol of our GPSM scheme relying on CI TPC may be formulated as:

$$e_{ant}^s \leq e_{ant}^{s,ub} = 1 - \int_0^\infty \left\{ \int_0^\infty [F_{\chi_2^2}(g)]^{N_r - N_a} f_{\chi_2^2}(g; \lambda) dg \right\}^{N_a} f_\lambda(\lambda) d\lambda, \quad (25)$$

where $F_{\chi_2^2}(g)$ represents the Cumulative Distribution Function (CDF) of a chi-square distribution having two degrees of freedom, while $f_{\chi_2^2}(g; \lambda)$ represents the Probability Distribution Function (PDF) of a non-central chi-square distribution having two degrees of freedom and non-centrality given by

$$\lambda = \frac{\beta}{N_a \sigma_0^2}, \quad (26)$$

with its PDF of $f_\lambda(\lambda)$ and $\sigma_0^2 = \sigma^2/2$. Finally, equality of (25) holds when $N_a = 1$.

Moreover, the PDF of $f_\lambda(\lambda)$ is formulated in Lemma III.3 and Lemma III.4, respectively, when either the loose or stringent power-normalisation factor of (4) and (5) is employed.

Lemma III.3 (Proof in Appendix C): When CI TPC is employed and the loose power-normalisation factor of (4) is used, the distribution $f_\lambda(\lambda)$ of the non-centrality λ is given by:

$$f_\lambda(\lambda) = \frac{2N_r}{\lambda^2 N_a \sigma^2} f_U\left(\frac{2N_r}{\lambda N_a \sigma^2}\right), \quad (27)$$

where by letting $U = \text{Tr}[(\mathbf{H}\mathbf{H}^H)^{-1}]$, we have $f_U(\cdot)$, which constitutes the derivative of $F_U(\cdot)$ and it is given in (50) of Appendix C.

Lemma III.4. (Proof in Appendix D): When CI TPC is employed and the stringent power-normalisation factor of (5) is used, the distribution $f_\lambda(\lambda)$ of the non-centrality λ is given by:

$$f_\lambda(\lambda) = \frac{N_a^{N_t - N_r + 1} \sigma^2 / 2}{(N_t - N_r)!} e^{-\lambda N_a \sigma^2 / 2} \left(\frac{\lambda \sigma^2}{2}\right)^{N_t - N_r}. \quad (28)$$

301 3) *Upper Bound of \tilde{e}_{mod}^s* : Considering a general case of
 302 N_r as well as N_a and assuming that the RA pattern $\mathcal{C}(k)$ was
 303 activated, after substituting (3) into (6), we have:

$$y_{v_i} = \sqrt{\beta/N_a} b_{m_i} + w_{v_i}, \quad \forall v_i \in \mathcal{C}(k), \quad (29)$$

$$y_{u_i} = w_{u_i}, \quad \forall u_i \in \bar{\mathcal{C}}(k), \quad (30)$$

304 where $\bar{\mathcal{C}}(k)$ denotes the complementary set of the activated RA
 305 pattern $\mathcal{C}(k)$ in \mathcal{C} . Hence, we have the signal to noise ratio
 306 (SNR) given as

$$\gamma = \gamma_{v_i} = \frac{\beta}{N_a \sigma^2} = \frac{\lambda}{2}, \quad \forall v_i \quad (31)$$

307 and for the remaining deactivated RAs in $\bar{\mathcal{C}}(k)$, we have only
 308 random noises of zero mean and variance of σ^2 .

309 The SER e_{mod}^s of the conventional modulated symbol $b_{m_i} \in$
 310 \mathcal{A} in the *absence* of spatial symbol errors may be upper
 311 bounded by [24]:

$$e_{\text{mod}}^s < N_{\min} \int_0^\infty \mathcal{Q}(d_{\min} \sqrt{\gamma/2}) f_\gamma(\gamma) d\gamma = e_{\text{mod}}^{s,ub}, \quad (32)$$

312 where in general $f_\gamma(\gamma)$ has to be acquired by the empirical
 313 histogram based method. When Lemma III.3 or Lemma III.4
 314 is exploited, $f_\gamma(\gamma)$ is a scaled version of $f_\lambda(\lambda)$, i.e. we have
 315 $f_\gamma(\gamma) = 2f_\lambda(2\gamma)$. Moreover, d_{\min} is the minimum Euclidean
 316 distance in the conventional modulated symbol constellation,
 317 N_{\min} is the average number of the nearest neighbours separated
 318 by d_{\min} in the constellation and $\mathcal{Q}(\cdot)$ denotes the Gaussian
 319 \mathcal{Q} -function.

320 When taking into account of the spatial symbol errors, we
 321 have Lemma III.5 for the upper bound of \tilde{e}_{mod}^s .

322 *Lemma III.5. (Proof in Appendix E)*: Given the k th activated
 323 RA patten, the SER of the conventional modulated symbols in
 324 the *presence* of spatial symbol errors can be upper bounded by:

$$\tilde{e}_{\text{mod}}^s < \left(1 - e_{\text{ant}}^{s,ub}\right) e_{\text{mod}}^{s,ub} + e_{\text{ant}}^{s,ub} \sum_{\ell \neq k} \frac{N_c e_{\text{mod}}^{s,ub} + N_d e_o^s}{N_a (2^{k_{\text{ant}}} - 1)} = \tilde{e}_{\text{mod}}^{s,ub}, \quad (33)$$

325 where N_c and $N_d = (N_a - N_c)$ represent the number of com-
 326 mon and different RA between $\mathcal{C}(\ell)$ and $\mathcal{C}(k)$, respectively.
 327 Mathematically we have $N_c = \sum_{i=1}^{N_a} \mathbb{I}[\mathcal{C}(\ell, i) \in \mathcal{C}(k)]$. More-
 328 over, $e_o^s = (M - 1)/M$ is SER as a result of random guess.

329 4) *Upper Bound of e_{eff}^s and e_{eff}^b* : By substituting (25) and
 330 (33) into (19) and (20), we arrive at the upper bound of the
 331 average symbol and bit error probability as

$$e_{\text{eff}}^{s,ub} = \frac{(e_{\text{ant}}^{s,ub} + N_a \tilde{e}_{\text{mod}}^{s,ub})}{(1 + N_a)} \quad (34)$$

$$e_{\text{eff}}^{b,ub} = \frac{(\delta_{\text{ant}} e_{\text{ant}}^{s,ub} + N_a \tilde{e}_{\text{mod}}^{s,ub})}{k_{\text{eff}}}. \quad (35)$$

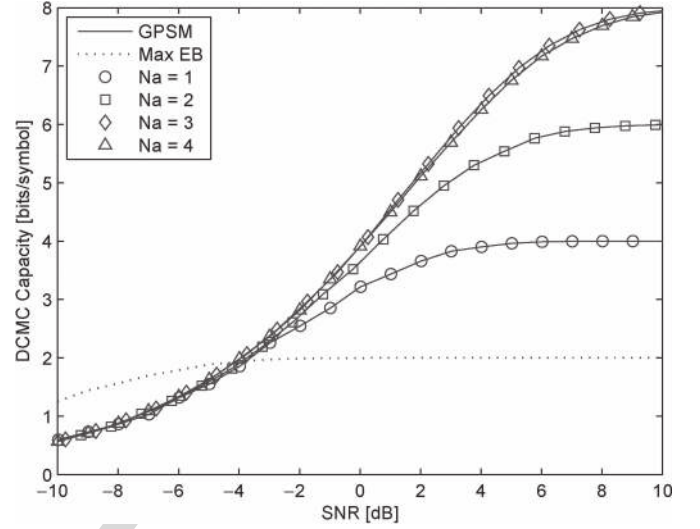


Fig. 1. DCMC capacity versus the SNR of the CI TPC aided GPSM scheme based on the loose power-normalisation factor of (4) under $\{N_t, N_r\} = \{8, 4\}$ and employing QPSK, while having $N_a = \{1, 2, 3, 4\}$ activated RAs.

Similarly, by substituting (25) and (33) into (24), we obtain the
 lower bound of the achievable rate as

$$R^{lb} = k_{\text{ant}} I \left(\delta_{k_{\text{ant}}} \frac{e_{\text{ant}}^{s,ub}}{k_{\text{ant}}} \right) + N_a k_{\text{mod}} I \left(\frac{\tilde{e}_{\text{mod}}^{s,ub}}{k_{\text{mod}}} \right). \quad (36)$$

IV. NUMERICAL RESULTS

We now provide numerical results for characterizing both the
 DCMC capacity of our GPSM scheme and for demonstrating
 the accuracy of our analytical error probability results.

A. DCMC Capacity

1) *Effect of the Number of Activated RAs*: Fig. 1 charac-
 terises the DCMC capacity versus the SNR of the CI TPC
 aided GPSM scheme based on the loose power-normalisation
 factor of (4) under $\{N_t, N_r\} = \{8, 4\}$ and employing QPSK,
 while having $N_a = \{1, 2, 3, 4\}$ activated RAs. It can be ob-
 served in Fig. 1 that the larger N_a , the higher the capacity of
 our GPSM scheme. Importantly, both the GPSM scheme of
 $N_a = 3$ marked by the diamonds and its conventional MIMO
 counterpart of $N_a = 4$ marked by the triangles attain the same
 ultimate DCMC capacity of 8 bits/symbol at a sufficiently high
 SNR, albeit the former exhibits a slightly higher capacity before
 reaching the 8 bits/symbol value. Furthermore, the DCMC ca-
 pacity of the conventional Maximal Eigen-Beamforming (Max
 EB) scheme is also included as a benchmark under $\{N_t, N_r\} =$
 $\{8, 4\}$ and employing QPSK, which exhibits a higher DCMC
 capacity at low SNRs, while only supporting 2 bits/symbol
 at most.

We further investigate the attainable bandwidth efficiency by
 replacing the SNR used in Fig. 1 by the SNR per bit in Fig. 2,
 where we have $\text{SNR}_b[\text{dB}] = \text{SNR}[\text{dB}] - 10 \log_{10}(C/N_a)$. It
 can be seen from Fig. 2 that the lower N_a , the higher the
 bandwidth efficiency attained in the low range of SNR_b . Im-
 portantly, the achievable bandwidth efficiency of $N_a = 3$ is

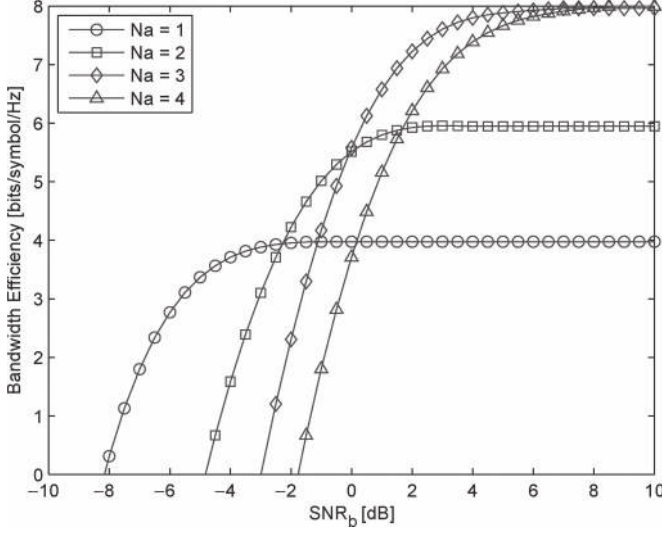


Fig. 2. Bandwidth efficiency versus the SNR_b of CI TPC aided GPSM scheme with the loose power-normalisation factor of (4) under $\{N_t, N_r\} = \{8, 4\}$ and employing QPSK, while having $N_a = \{1, 2, 3, 4\}$ activated RAs.

362 consistently and significantly higher than that achieved by
 363 $N_a = 4$, before they both converge to 8 bits/symbol/Hz at their
 364 maximum. Overall, there is always a beneficial configuration
 365 for our GPSM scheme that offers the same bandwidth efficiency
 366 as that of its conventional MIMO counterpart, which is achieved
 367 at a lower SNR per bit.

368 2) *Robustness to Impairments*: Like in all TPC schemes,
 369 an important aspect related to GPSM is its resilience to CSIT
 370 inaccuracies. In this paper, we let $\mathbf{H} = \mathbf{H}_a + \mathbf{H}_i$, where \mathbf{H}_a
 371 represents the matrix hosting the average CSI, with each entry
 372 obeying the complex Gaussian distribution of $h_a \sim \mathcal{CN}(0, \sigma_a^2)$
 373 and \mathbf{H}_i is the instantaneous CSI error matrix obeying the
 374 complex Gaussian distribution of $h_i \sim \mathcal{CN}(0, \sigma_i^2)$, where we
 375 have $\sigma_a^2 + \sigma_i^2 = 1$. As a result, only \mathbf{H}_a is available at the
 376 transmitter for pre-processing.

377 Another typical impairment is antenna correlation. The
 378 correlated MIMO channel is modelled by the widely-used
 379 Kronecker model, which is written as $\mathbf{H} = (\mathbf{R}_t^{1/2})\mathbf{G}(\mathbf{R}_r^{1/2})^T$,
 380 with \mathbf{G} representing the original MIMO channel imposing no
 381 correlation, while \mathbf{R}_t and \mathbf{R}_r represents the correlations at the
 382 transmitter and receiver side, respectively, with the correlation
 383 entries given by $R_t(i, j) = \rho_t^{|i-j|}$ and $R_r(i, j) = \rho_r^{|i-j|}$.

384 Figs. 3 and 4 characterise the effect of imperfect CSIT
 385 associated with $\sigma_i = 0.4$ and of antenna correlation of $\rho_t =$
 386 $\rho_r = 0.3$ on the attainable DCMC capacity versus the SNR
 387 for our CI TPC aided GPSM scheme with the loose power-
 388 normalisation factor of (4), respectively, under $\{N_t, N_r\} =$
 389 $\{8, 4\}$ and employing QPSK having $N_a = \{1, 2, 3, 4\}$ activated
 390 RAs. It can be seen that as expected, both impairments result
 391 into a degraded DCMC capacity. Observe in Fig. 3 for im-
 392 perfect CSIT that the degradation of the conventional MIMO
 393 associated with $N_a = 4$ and marked by the triangle is larger
 394 than that of our GPSM scheme corresponding $N_a = \{1, 2, 3\}$.
 395 On the other hand, as seen in Fig. 4, roughly the same level of
 396 degradation is observed owing to antenna correlation.

397 3) *Effect of Modulation Order and MIMO Configuration*:
 398 Fig. 5 characterises the DCMC capacity versus the SNR

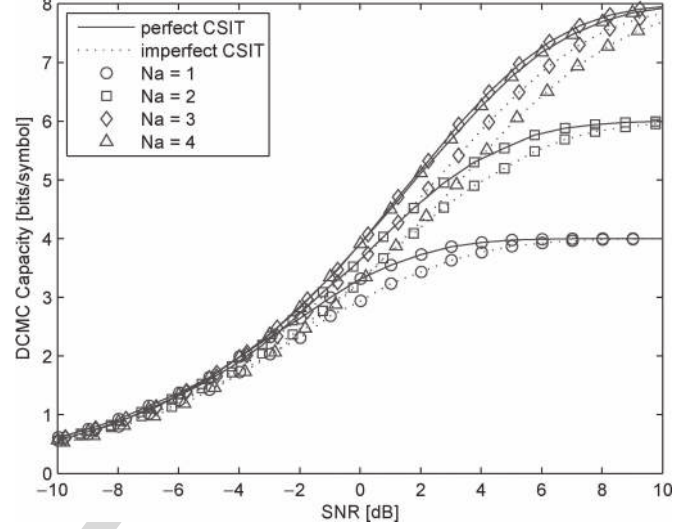


Fig. 3. The effect of imperfect CSIT with $\sigma_i = 0.4$ on the DCMC capacity versus the SNR of CI TPC aided GPSM scheme with the loose power-normalisation factor of (4) under $\{N_t, N_r\} = \{8, 4\}$ and employing QPSK having $N_a = \{1, 2, 3, 4\}$ activated RAs.

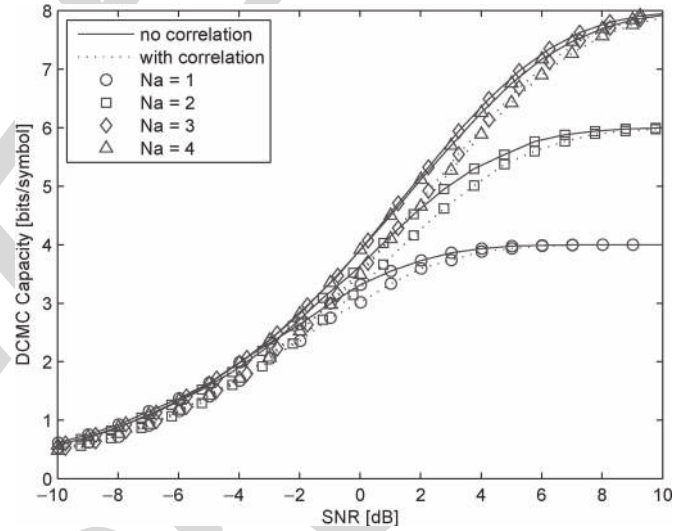


Fig. 4. The effect of antenna correlation with $\rho_t = \rho_r = 0.3$ on the DCMC capacity versus the SNR of CI TPC aided GPSM scheme with the loose power-normalisation factor of (4) under $\{N_t, N_r\} = \{8, 4\}$ and employing QPSK having $N_a = \{1, 2, 3, 4\}$ activated RAs.

of our CI TPC aided GPSM scheme relying on the loose
 power-normalisation factor of (4) under $\{N_t, N_r\} = \{8, 4\}$ and
 employing various conventional modulation schemes having
 $N_a = \{1, 2\}$ activated RAs. It can be seen that the higher the
 modulation order M , the higher the achievable DCMC capac-
 ity. Furthermore, for a fixed modulation order M , the higher
 the value of N_a , the higher the achievable DCMC capacity
 becomes as a result of the information embedded in the spatial
 symbol.

Fig. 6 characterises the DCMC capacity versus the SNR
 for our CI TPC aided GPSM scheme for the loose power-
 normalisation factor of (4) under different settings of $\{N_t, N_r\}$
 with $N_t/N_r = 2$ and employing QPSK, while having $N_a =$
 $\{1, 2\}$ activated RAs. It can be seen in Fig. 6 that for a fixed
 MIMO setting, the higher the value of N_a , the higher the

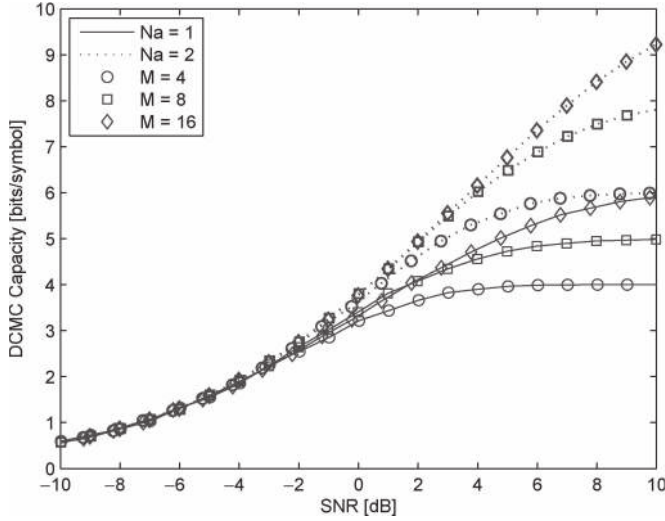


Fig. 5. DCMC capacity versus the SNR of our CI TPC aided GPSM scheme relying on the loose power-normalisation factor of (4) under $\{N_t, N_r\} = \{8, 4\}$ and employing various conventional modulation schemes having $N_a = \{1, 2\}$ activated RAs.

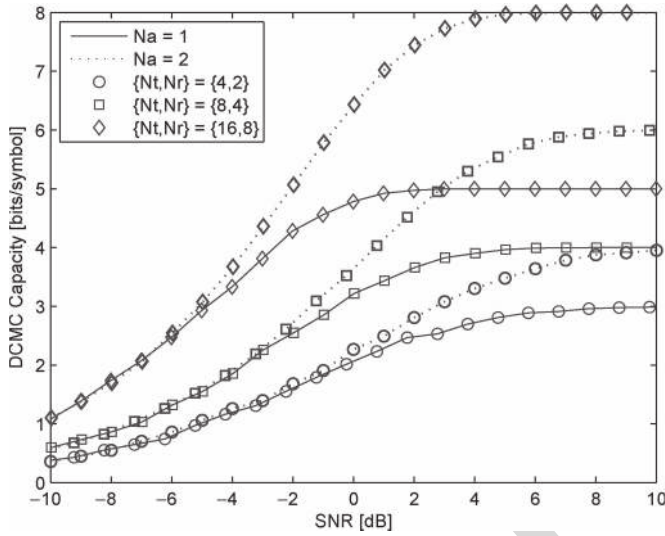


Fig. 6. DCMC capacity versus the SNR for our CI TPC aided GPSM scheme for the loose power-normalisation factor of (4) under different settings of $\{N_t, N_r\}$ with $N_t/N_r = 2$ and employing QPSK, while having $N_a = \{1, 2\}$ activated RAs.

414 DCMC capacity becomes. Importantly, for a fixed N_a , the
415 larger the size of the MIMO antenna configuration, the higher
416 the DCMC capacity.

417 B. Achievable Rate

418 1) *Error Probability*: Figs. 7–10 characterize the GPSM
419 scheme's SER as well as the BER under both the loose
420 power-normalisation factor of (4) and the stringent power-
421 normalisation factor of (5) for $\{N_t, N_r\} = \{16, 8\}$ and em-
422 ploying QPSK, respectively. From Figs. 7–10, we recorded the
423 curves from left to right corresponding to $N_a = \{1, 2, 4, 6\}$. For
424 reasons of space-economy and to avoid crowded figures, our
425 results for $N_a = \{3, 5, 7\}$ were not shown here, but they obey
426 the same trends.

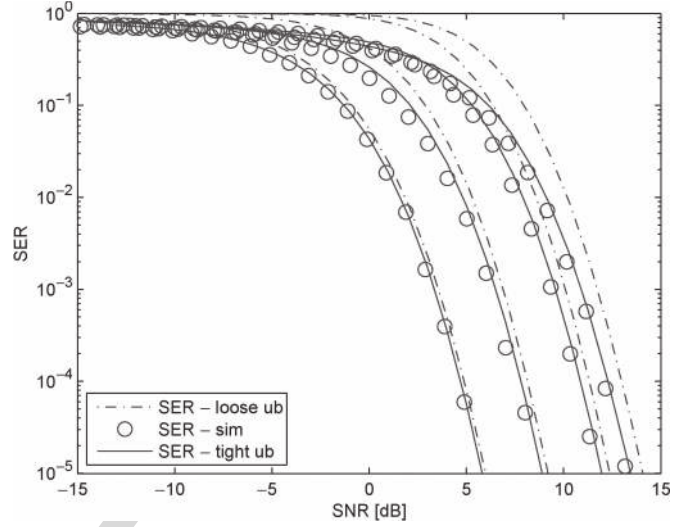


Fig. 7. GPSM scheme's SER with CI TPC and the **loose** power-normalisation factor of (4) under $\{N_t, N_r\} = \{16, 8\}$ and employing QPSK. Curves from left to right correspond to $N_a = \{1, 2, 4, 6\}$.

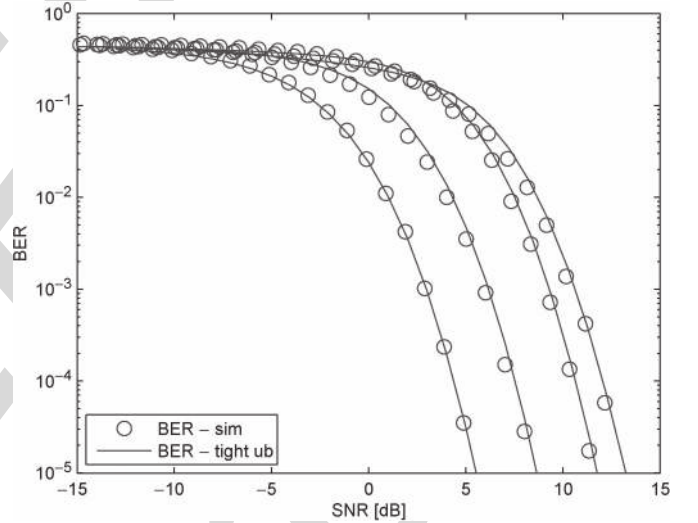


Fig. 8. GPSM scheme's BER with CI TPC and the **loose** power-normalisation factor of (4) under $\{N_t, N_r\} = \{16, 8\}$ and employing QPSK. Curves from left to right correspond to $\{N_a = 1, 2, 4, 6\}$.

It can be seen from Figs. 7 and 9 that our analytical SER
results of (34) form tight upper bounds for the empirical sim-
ulation results. Hence they are explicitly referred to as 'tight
upper bound' in both figures. Additionally, a loose upper bound
of the GPSM scheme's SER is also included, which may be
written as

$$e_{eff}^{s, lub} = 1 - \left(1 - e_{ant}^{s, ub}\right) \left(1 - e_{mod}^{s, ub}\right). \quad (37)$$

Note that in this loose upper bound expression, $e_{mod}^{s, ub}$ of (32) is
required rather than $\tilde{e}_{mod}^{s, ub}$ of (33). This expression implicitly
assumes that the detection of (8) and (9) are independent.
However, the first-step detection of (8) significantly affects the
second-step detection of (9). Hence, the loose upper bound
shown by the dash-dot line is only tight for $N_a = 1$ and
becomes much looser upon increasing N_a , when compared to
the tight upper bound of (34).

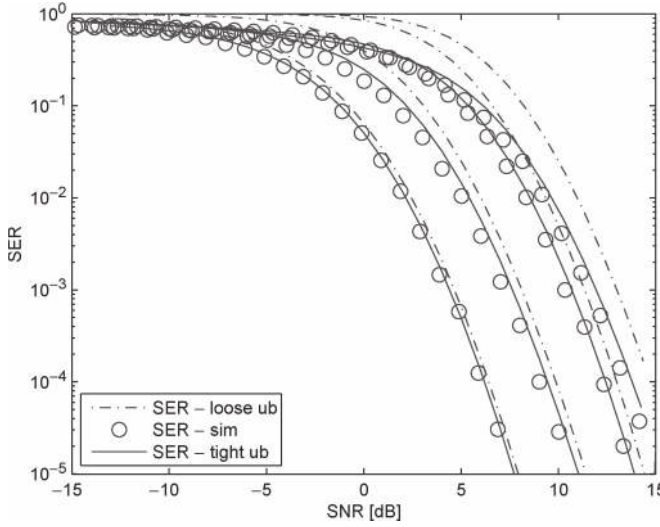


Fig. 9. GPSM scheme's SER with CI TPC and the **stringent** power-normalisation factor of (5) under $\{N_t, N_r\} = \{16, 8\}$ and employing QPSK. Curves from left to right correspond to $N_a = \{1, 2, 4, 6\}$.

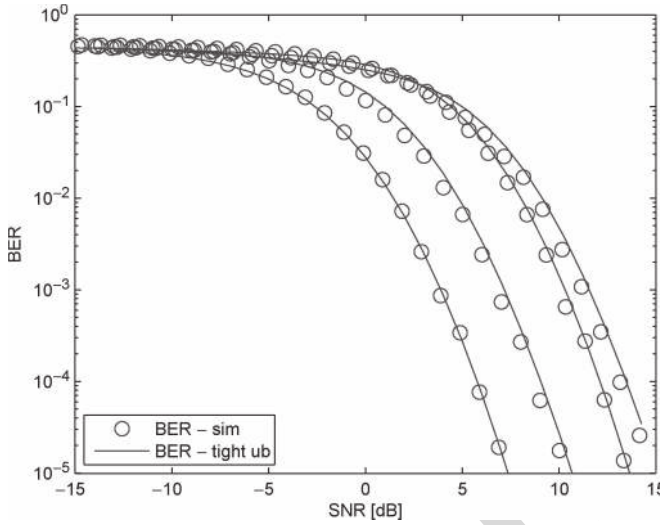


Fig. 10. GPSM scheme's BER with CI TPC and the **stringent** power-normalisation factor of (5) under $\{N_t, N_r\} = \{16, 8\}$ and employing QPSK. Curves from left to right correspond to $\{N_a = 1, 2, 4, 6\}$.

441 Similarly, when the GPSM scheme's BER is considered in
442 Figs. 8 and 10, our analytical results of (35) again form
443 tight upper bounds for the empirical results.

444 2) *Separability*: To access the inner nature of first-step de-
445 tection of (8), Fig. 11 reveals the separability between the
446 activated RAs and deactivated RAs in our GPSM scheme,
447 where the PDF of (44) and (45) were recorded both for SNR =
448 -5 dB (left subplot) and for SNR = 0 dB (right subplot)
449 respectively for the same snapshot of MIMO channel realisation
450 with the aid of CI TPC and the loose power-normalisation factor
451 of (4) under $\{N_t, N_r\} = \{16, 8\}$ and employing QPSK. By
452 comparing the left subplot to the right subplot, it becomes clear
453 that the higher the SNR, the better the separability between the
454 activated and the deactivated RAs, since the mean of the solid
455 curves representing (44) move further apart from that of the
456 dashed curve representing (45). Furthermore, as expected, the

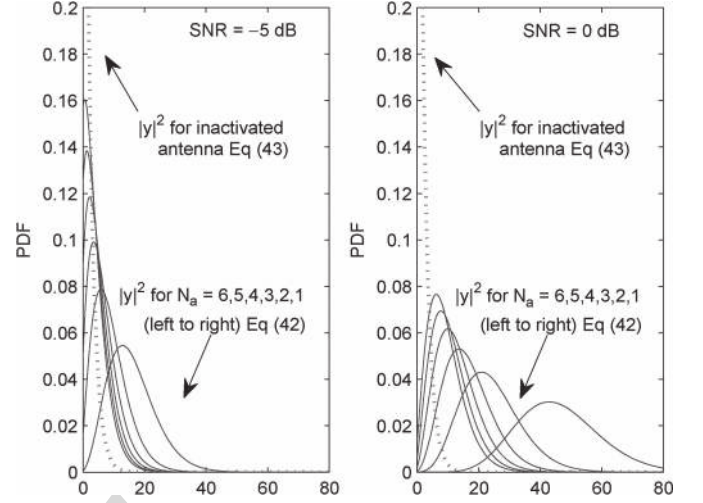


Fig. 11. The PDF of (44) and (45) under both SNR = -5 dB (left) and SNR = 0 dB (right) for the same snapshot of MIMO channel realisation with CI TPC and the loose power-normalisation factor of (4) under $\{N_t, N_r\} = \{16, 8\}$ and employing QPSK.

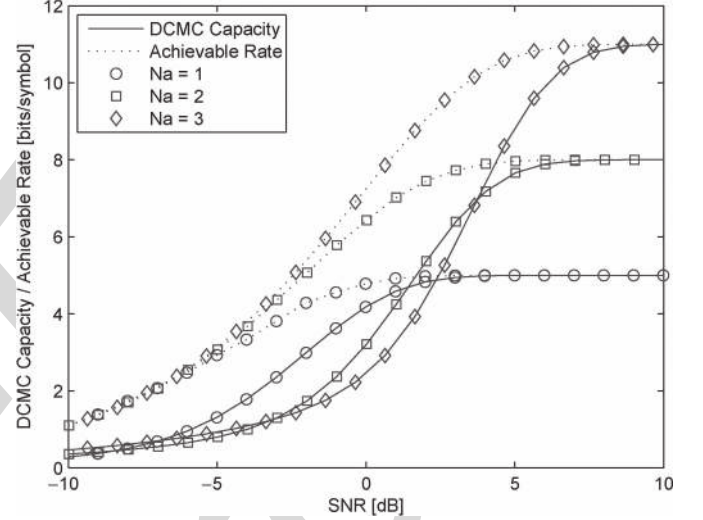


Fig. 12. Comparison between the DCMC capacity of our GPSM scheme relying implicitly on the ML-based joint detection and its lower bound of the achievable rate relying on the low-complexity decoupled detection, where we use CI TPC with the loose power-normalisation factor of (4) under $\{N_t, N_r\} = \{16, 8\}$ and employing QPSK having $N_a = \{1, 2, 3\}$.

457 lower N_a , the better the separability becomes, as demonstrated
458 in both subplots of Fig. 11.

459 3) *Comparison*: Finally, Fig. 12 characterizes the compar-
460 ison between the DCMC capacity (14) of our GPSM scheme
461 relying implicitly on the ML-based joint detection of (7) and
462 its lower bound of the achievable rate in (36) relying on the
463 low-complexity decoupled detection of (8) and (9), where we
464 use CI TPC with the loose power-normalisation factor of (4)
465 under $\{N_t, N_r\} = \{16, 8\}$ and employing QPSK having $N_a =$
466 $\{1, 2, 3\}$.

It is clear that the DCMC capacity is higher than the
achievable rate for each N_a considered, although both of them
converge to the same value, when the SNR is sufficiently high.
Noticeably, the discrepancy between the two quantities before
their convergence is wider, when N_a is higher. This is because
the higher N_a , the lower the achievable rate at low SNRs,

473 which is shown by comparing the solid curves. This echoes
 474 our observations of Fig. 11, namely that a higher N_a leads
 475 to a reduced separability and consequently both to a higher
 476 overall error probability and to a lower achievable rate. In
 477 fact, the achievable rate becomes especially insightful after
 478 being compared to the DCMC capacity, where we may tell
 479 how a realistic decoupled detection performs and how far its
 480 performance is from the DCMC capacity.

481 V. CONCLUSION

482 In this paper, we introduced the concept of our GPSM
 483 scheme and carried out its theoretical analysis in terms of both
 484 its DCMC capacity as well as its achievable rate relying on our
 485 analytical upper bound of the SER and the BER expressions,
 486 when a low-complexity decoupled detector is employed. Our
 487 numerical results demonstrate that the upper bound introduced
 488 is tight and the DCMC capacity analysis indicates that our
 489 GPSM scheme constitutes a flexible MIMO arrangement. Our
 490 future work will consider a range of other low-complexity
 491 MIMO schemes, such as the receive antenna selection and the
 492 classic SM, in the context of large-scale MIMOs.

493 Furthermore, the insights of our error probability and capac-
 494 ity analysis are multi-folds:

- 495 • It can be seen that there is a gap between the DCMC
 496 capacity relying on ML detection and the achievable rate
 497 of decoupled detection. Thus, a novel detection method is
 498 desired for closing this gap and for striking a better trade-
 499 off between the performance attained and the complexity
 500 imposed.
- 501 • The error probability derived serves as a tight upper bound
 502 of our GPSM performance. This facilitates the convenient
 503 study of finding beneficial bit-to-symbol mapping and
 504 error-probability balancing between the spatial symbols
 505 and conventional modulated symbols [25]. Otherwise,
 506 excessive-complexity bit-by-bit Monte-Carlo simulations
 507 would be required.
- 508 • Furthermore, both the capacity and error probability anal-
 509 ysis provide a bench-marker for conducting further re-
 510 search on antenna selection techniques for our GPSM
 511 scheme, where different criteria may be adopted either
 512 for maximizing the capacity or for minimizing the error
 513 probability, again without excessive-complexity bit-by-bit
 514 Monte-Carlo simulations.

515 APPENDIX A

516 PROOF OF LEMMA III.1

517 Let $\mathcal{A}_{k_{ant}}$ denote the alphabet of the spatial symbol having
 518 k_{ant} bits of information. Then the cardinality of the alphabet
 519 $\mathcal{A}_{k_{ant}}$ is twice higher compared to that of $\mathcal{A}_{k_{ant}-1}$. Thus,
 520 $\mathcal{A}_{k_{ant}}$ may be constructed by two sub-alphabets of $\mathcal{A}_{k_{ant}-1}$,
 521 represented by 0 and 1, respectively. We may thereafter refer to
 522 the alphabet of $\mathcal{A}_{k_{ant}-1}$ preceded by the above-mentioned with
 523 0 (1) as zero-alphabet (one-alphabet).

524 Assuming that the spatial symbol representing k_{ant} zeros
 525 was transmitted, we may then calculate the total number of
 526 pair-wise bit errors ϵ_0 in the above zero-alphabet. Hence, the

number of pair-wise bit errors ϵ_1 in the one-alphabet is simply
 $\epsilon_1 = \epsilon_0 + A$, where $A = 2^{k_{ant}}$ accounts for the difference in
 the first preceding bit. Hence the total number of pair-wise
 bit errors is $\epsilon = 2\epsilon_0 + 2^{k_{ant}}$. Taking into account an equal
 probability of $1/(2^{k_{ant}} - 1)$ for each possible spatial symbol
 error, we arrive at the correction factor given by $\delta_{k_{ant}} = (2\epsilon_0 + 2^{k_{ant}})/(2^{k_{ant}} - 1)$.

Since ϵ_0 represents the total number of pair-wise bit errors
 corresponding to case of $(k_{ant} - 1)$ bits of information, we
 have $\epsilon_0 = (2^{k_{ant}-1} - 1)\delta_{k_{ant}-1}$. Hence the resultant expres-
 sion of the correction factor may be calculated recursively
 according to (23) after some further manipulations.³

APPENDIX B

PROOF OF LEMMA III.2

Considering a general case of N_r as well as N_a and assuming
 that the RA pattern $\mathcal{C}(k)$ was activated, after substituting (3)
 into (6), we have:

$$y_{v_i} = \sqrt{\beta/N_a} b_{m_i} + w_{v_i}, \quad \forall v_i \in \mathcal{C}(k), \quad (38)$$

$$y_{u_i} = w_{u_i}, \quad \forall u_i \in \bar{\mathcal{C}}(k), \quad (39)$$

where $\bar{\mathcal{C}}(k)$ denotes the complementary set of the activated RA
 pattern $\mathcal{C}(k)$ in \mathcal{C} . Furthermore, upon introducing $\sigma_0^2 = \sigma^2/2$,
 we have:

$$|y_{v_i}|^2 = \mathcal{R}(y_{v_i})^2 + \mathcal{I}(y_{v_i})^2 \quad (40)$$

$$\sim \mathcal{N}\left(\sqrt{\beta/N_a} \mathcal{R}(b_{m_i}), \sigma_0^2\right) + \mathcal{N}\left(\sqrt{\beta/N_a} \mathcal{I}(b_{m_i}), \sigma_0^2\right), \quad (41)$$

$$|y_{u_i}|^2 = \mathcal{R}(w_{u_i})^2 + \mathcal{I}(w_{u_i})^2 \quad (42)$$

$$\sim \mathcal{N}(0, \sigma_0^2) + \mathcal{N}(0, \sigma_0^2), \quad (43)$$

where $\mathcal{R}(\cdot)$ and $\mathcal{I}(\cdot)$ represent the real and imaginary operators,
 respectively. As a result, by normalisation with respect to σ_0^2 ,
 we have the following observations:

$$|y_{v_i}|^2 \sim \chi_2^2(g; \lambda_{v_i}), \quad \forall v_i \in \mathcal{C}(k), \quad (44)$$

$$|y_{u_i}|^2 \sim \chi_2^2(g), \quad \forall u_i \in \bar{\mathcal{C}}(k), \quad (45)$$

where the non-centrality is given by $\lambda_{v_i} = \beta|b_{m_i}|^2/N_a\sigma_0^2$.
 Exploiting the fact that $\mathbb{E}[|b_{m_i}|^2] = 1$, $\forall i$ (or $|b_{m_i}|^2 = 1$, $\forall i$ for
 PSK modulation), we have $\lambda = \lambda_{v_i}$, $\forall v_i$. Note that λ is also a
 random variable obeying the distribution of $f_\lambda(\lambda)$.

Recall from (8) that the correct decision concerning the
 spatial symbols occurs, when $\sum_{i=1}^{N_a} |y_{v_i}|^2$ is the maximum.
 By exploiting the fact that $\mathbb{E}_{\mathcal{C}(k)}[\Delta] = \Delta$, the correct detection
 probability Δ of the spatial symbols given the non-centrality λ ,

³By assuming equal-probability erroneously detected patterns, a spatial
 symbol may be mistakenly detected as any of the other spatial symbols with
 equal probability. Let us now give an example for highlighting the rationale
 of introducing the correction factor. For example, spatial symbol '0' carrying
 bits [0,0] was transmitted, it would result into a one-bit difference when the
 spatial symbol '1' carrying [0,1] or '2' carrying [1,0] was erroneously detected.
 However, it would result into a two-bits difference when spatial symbol '3'
 carrying [1,1] was erroneously detected. This corresponds to four bit errors
 in total for these three cases, thus a correction factor of 4/3 is needed when
 converting the symbol error ratio to bit error ratio.

when the RA pattern $\mathcal{C}(k)$ was activated may be lower bounded as in (46). (See equation at bottom of page) More explicitly,

- equation (a) serves as the lower bound, since it sets the most strict condition for the correct detection, when each metric y_{u_j} of the inactivated RA indices in $\bar{\mathcal{C}}(k)$ is lower than each metric g_{v_i} of the activated RA indices in $\mathcal{C}(k)$. Note that, equality holds when $N_a = 1$;
- equation (b) follows from the fact that the N_a random variables $|y_{v_i}|^2$ are independent of each other;
- equation (c) follows from the fact that the $(N_r - N_a)$ random variables $|y_{u_j}|^2$ are independent and equation (d) follows from the fact that the N_a independent variables of $|y_{v_i}|^2$ and the $(N_r - N_a)$ independent variables of $|y_{u_j}|^2$ are both identically distributed.

As a result, after averaging over the distribution of $f_\lambda(\lambda)$, the analytical SER e_{ant}^s of the spatial symbol in our GPSM scheme may be upper bounded as in (25). In general, the expression of $f_\lambda(\lambda)$ can be acquired with the aid of the empirical histogram based method, while in case the loose/stringent power-normalisation factor of (4)/(5) is used, the analytical expression for $f_\lambda(\lambda)$ is given in Lemma III.3/Lemma III.4.

APPENDIX C

PROOF OF LEMMA III.3

Upon expanding the expression of λ in (26) by taking into account (4), we have:

$$\lambda = \frac{\beta_l}{N_a \sigma_0^2} = \frac{N_r}{N_a \sigma_0^2 \text{Tr}[(\mathbf{H}\mathbf{H}^H)^{-1}]}. \quad (47)$$

Consider first the distribution of $\text{Tr}[(\mathbf{H}\mathbf{H}^H)^{-1}]$ and let $\mathbf{W} = \mathbf{H}\mathbf{H}^H$. Since the entries of \mathbf{H} are i.i.d. zero-mean unit-

variance complex Gaussian random variables, \mathbf{W} obeys a complex Wishart distribution. Hence the joint PDF of its eigenvalues $\{\lambda_{\mathbf{W}_i}\}_{i=1}^{N_r}$ is given by [26], [27]

$$f_{\mathbf{W}}(\{\lambda_{\mathbf{W}_i}\}_{i=1}^{N_r}) = \frac{K^{-1}}{N_r!} \prod_i e^{-\lambda_{\mathbf{W}_i}} \lambda_{\mathbf{W}_i}^{N_t - N_r} \prod_{i < j} (\lambda_{\mathbf{W}_i} - \lambda_{\mathbf{W}_j})^2, \quad (48)$$

where K is a normalising factor. Thus for its inverse $\mathbf{U} = \mathbf{W}^{-1}$, we have

$$f_{\mathbf{U}}(\{\lambda_{\mathbf{U}_i}\}_{i=1}^{N_r}) = \prod_i \lambda_{\mathbf{U}_i}^{-2} f_{\mathbf{W}}(\{\lambda_{\mathbf{W}_i}^{-1}\}_{i=1}^{N_r}). \quad (49)$$

Furthermore, since $\text{Tr}[\mathbf{U}] = \sum \lambda_{\mathbf{U}_i}$, where $\{\lambda_{\mathbf{U}_i}\}_{i=1}^{N_r}$ is the eigenvalues of \mathbf{U} , we have the CDF of $\text{Tr}[\mathbf{U}]$ given by (50), where $T_1 = T$ and $t_1 = 1/T$, while $\forall j > 1$

$$T_j = T - \sum_{i=1}^{j-1} \lambda_{\mathbf{U}_i}, \quad \frac{t_j - 1}{\left(T - \sum_{i=1}^{j-1} \lambda_{\mathbf{U}_i}^{-1}\right)}.$$

Let $\lambda_0 = 1/\text{Tr}[\mathbf{U}]$. Then, from the above analysis we know that the PDF of $f_{\text{Tr}[\mathbf{U}]}$ is the derivative of (50). (See equation at the bottom of the page) Hence, we may also get the PDF of $f_{\lambda_0}(\lambda_0) = \lambda_0^{-2} f_{\text{Tr}[\mathbf{U}]}(\lambda_0^{-1})$. Finally, since $\lambda_0 = \lambda N_a \sigma_0^2 / N_r$, we have $f_\lambda(\lambda) = N_a \sigma_0^2 f_{\lambda_0}(\lambda N_a \sigma_0^2 / N_r) / N_r$. After simple manipulations, we have (27).

APPENDIX D

PROOF OF LEMMA III.4

Upon expanding the expression of λ in (26) by taking into account (5), we have:

$$\lambda = \frac{\beta_s}{N_a \sigma_0^2} = \frac{1}{\sigma_0^2 \mathbf{s}^H (\mathbf{H}\mathbf{H}^H)^{-1} \mathbf{s}}. \quad (51)$$

$$\begin{aligned} \Delta &\stackrel{a}{\geq} \int_0^\infty P(|y_{u_1}|^2 < g_{v_1}, \dots, |y_{u_{N_r-N_a}}|^2 < g_{v_1}, \dots, |y_{u_1}|^2 < g_{v_{N_a}}, \dots, |y_{u_{N_r-N_a}}|^2 < g_{v_{N_a}}) \\ &\quad \cdot P(|y_{v_1}|^2 = g_{v_1}, \dots, |y_{v_{N_a}}|^2 = g_{v_{N_a}} | \lambda_{v_1}, \dots, \lambda_{v_{N_a}}) dg_{v_1} \cdots dg_{v_{N_a}} \\ &\stackrel{b}{=} \prod_{i=1}^{N_a} \int_0^\infty P(|y_{u_1}|^2 < g_{v_i}, \dots, |y_{u_{N_r-N_a}}|^2 < g_{v_i}) P(|y_{v_i}|^2 = g_{v_i} | \lambda_{v_i}) dg_{v_i} \\ &\stackrel{c}{=} \prod_{i=1}^{N_a} \int_0^\infty \prod_{u_j \in \bar{\mathcal{C}}(k)} P(|y_{u_j}|^2 < g_{v_i}) P(|y_{v_i}|^2 = g_{v_i} | \lambda_{v_i}) dg_{v_i} \\ &\stackrel{d}{=} \left\{ \int_0^\infty [F_{\chi^2_2}(g)]^{N_r-N_a} f_{\chi^2_2}(g; \lambda) dg \right\}^{N_a} \end{aligned} \quad (46)$$

$$F_{\text{Tr}[\mathbf{U}]}(T) = \int_0^{T_1} \int_0^{T_2} \cdots \int_0^{T_{N_r}} f_{\mathbf{U}}(\{\lambda_{\mathbf{U}_i}\}_{i=1}^{N_r}) d\lambda_{\mathbf{U}_{N_r}} \cdots d\lambda_{\mathbf{U}_1} = \int_{t_1}^\infty \int_{t_2}^\infty \cdots \int_{t_{N_r}}^\infty f_{\mathbf{W}}(\{\lambda_{\mathbf{U}_i}^{-1}\}_{i=1}^{N_r}) d\lambda_{\mathbf{U}_{N_r}}^{-1} \cdots d\lambda_{\mathbf{U}_1}^{-1} \quad (50)$$

Since the entries of \mathbf{H} are i.i.d. zero-mean unit-variance complex Gaussian random variables, $\mathbf{H}\mathbf{H}^H$ obeys a complex Wishart distribution with N_r dimensions and $2N_t$ degrees of freedom, where we have:

$$\mathbf{H}\mathbf{H}^H \sim \mathcal{CW}(\Sigma, N_r, 2N_t), \quad (52)$$

with $\Sigma = (1/2)I_{N_r}$ being the variance. By exploiting proposition 8.9 from [28] and letting $\lambda_0 = [\mathbf{s}^H(\mathbf{H}\mathbf{H}^H)^{-1}\mathbf{s}]^{-1}$, we have:

$$\lambda_0 \sim \mathcal{CW}[(\mathbf{s}^H \Sigma^{-1} \mathbf{s})^{-1}, 1, 2(N_t - N_r + 1)], \quad (53)$$

where $A \sim B$ stands for A follows the distribution of B . According to [28], the above one-dimensional complex-valued Wishart distribution is actually a chi-square distribution with $2(N_t - N_r + 1)$ degrees of freedom and scaling parameter of $(\mathbf{s}^H \Sigma^{-1} \mathbf{s})^{-1} = 1/2N_a$. Thus, the PDF of λ_0 may be explicitly written as:

$$\begin{aligned} f_{\lambda_0}(\lambda_0) &= f_{\chi^2}[2N_a\lambda_0; 2(N_t - N_r + 1)] \\ &= 2N_a \frac{e^{-\lambda_0 N_a} (2N_a \lambda_0)^{N_t - N_r}}{2^{N_t - N_r + 1} (N_t - N_r)!} \\ &= \frac{N_a^{N_t - N_r + 1} e^{-\lambda_0 N_a} \lambda_0^{N_t - N_r}}{(N_t - N_r)!}. \end{aligned} \quad (54)$$

Finally, since $\lambda_0 = \sigma_0^2 \lambda$, we have $f_\lambda(\lambda) = \sigma_0^2 f_{\lambda_0}(\sigma_0^2 \lambda)$, which is (28).

APPENDIX E

PROOF OF LEMMA III.5

The SER of \tilde{e}_{mod}^s is constituted by the SER of e_{mod}^s , when the detection of the spatial symbol is correct having a probability of $(1 - e_{\text{ant}}^s)$, plus the SER, when the detection of the spatial symbol is erroneous having a probability of e_{ant}^s , which is expressed as

$$\begin{aligned} \tilde{e}_{\text{mod}}^s &\stackrel{a}{=} (1 - e_{\text{ant}}^s) e_{\text{mod}}^s \\ &\quad + e_{\text{ant}}^s \sum_{\ell \neq k} P_{k \rightarrow \ell} \underbrace{\frac{N_c e_{\text{mod}}^s + N_d e_o^s}{N_a}}_E, \\ &\stackrel{b}{<} (1 - e_{\text{ant}}^s) e_{\text{mod}}^{s,ub} \\ &\quad + e_{\text{ant}}^s \sum_{\ell \neq k} P_{k \rightarrow \ell} \frac{N_c e_{\text{mod}}^{s,ub} + N_d e_o^s}{N_a}, \\ &\stackrel{c}{\leq} (1 - e_{\text{ant}}^s) e_{\text{mod}}^{s,ub} \\ &\quad + \frac{e_{\text{ant}}^s}{(2^{k_{\text{ant}}} - 1)} \sum_{\ell \neq k} \frac{N_c e_{\text{mod}}^{s,ub} + N_d e_o^s}{N_a}, \\ &\stackrel{d}{\leq} (1 - e_{\text{ant}}^s) e_{\text{mod}}^{s,ub} \\ &\quad + e_{\text{ant}}^s \underbrace{\sum_{\ell \neq k} \frac{N_c e_{\text{mod}}^{s,ub} + N_d e_o^s}{N_a (2^{k_{\text{ant}}} - 1)}}_A = \tilde{e}_{\text{mod}}^{s,ub}. \end{aligned}$$

Regarding the second additive term of (a), the true activated RA pattern $\mathcal{C}(k)$ may be erroneously deemed to be any of the other

legitimate RA patterns $\mathcal{C}(\ell) \in \mathcal{C}, \ell \neq k$ with a probability of $P_{k \rightarrow \ell}$, which we have to average over. As for the calculation of the per-case error rates E , when $\mathcal{C}(k)$ was erroneously detected as a particular $\mathcal{C}(\ell)$, we found that it was constituted by the error rates of e_{mod}^s for those N_c RAs in common (which maybe regarded as being partially correctly detected) and the error rates of e_o^s for those RAs that were exclusively hosted by $\mathcal{C}(\ell)$, but were excluded from $\mathcal{C}(k)$. Furthermore, since only random noise may be received by those N_d RAs in $\mathcal{C}(\ell)$, thus e_o^s simply represents the SER as a result of a random guess, i.e. we have $e_o^s = (M - 1)/M$. Let us now provide some further detailed discussions of the relations ranging from (b) to (d):

- relation (b) holds true, since \tilde{e}_{mod}^s is a monotonic function of e_{mod}^s , thus it is upper bounded upon replacing e_{mod}^s by $e_{\text{mod}}^{s,ub}$;
- although it is natural that patterns with a higher N_c would be more likely to cause an erroneous detection, we assume an equal probability of $P_{k \rightarrow \ell} = 1/(2^{k_p} - 1)$. The equal probability assumption thus puts more weight on the patterns having higher N_d , since we have $e_o^s > e_{\text{mod}}^{s,ub}$. This leads to the relation of (c). Note that, equality holds when $N_a = 1$, where $N_c = 0$ and $N_d = 1$;
- replacing e_{ant}^s by $e_{\text{ant}}^{s,ub}$ puts more weight on the second additive term of (d), since having $e_o^s > e_{\text{mod}}^{s,ub}$ leads to the relation of $A > e_{\text{mod}}^{s,ub}$. As a result (d) also holds. Again, equality holds when $N_a = 1$, where $e_{\text{ant}}^s = e_{\text{ant}}^{s,ub}$ as indicated by Lemma III.2.

ACKNOWLEDGMENT

The financial support of the EPSRC under the India-UK Advanced Technology Centre (IU-ATC), that of the EU under the Concerto project as well as that of the European Research Council's (ERC) Advance Fellow Grant is gratefully acknowledged.

REFERENCES

- R. Zhang and L. Hanzo, "Wireless cellular networks," *IEEE Veh. Technol. Mag.*, vol. 5, no. 4, pp. 31–39, Dec. 2010.
- P. Wolniansky, G. Foschini, G. Golden, and R. Valenzuela, "V-BLAST: An architecture for realizing very high data rates over the rich-scattering wireless channel," in *Proc. URSI Int. Symp. Signals, Syst., Electron.*, 1998, pp. 295–300.
- S. Alamouti, "A simple transmit diversity technique for wireless communications," *IEEE J. Sel. Areas Commun.*, vol. 16, no. 8, pp. 1451–1458, Oct. 1998.
- Q. Spencer, C. Peel, A. Swindlehurst, and M. Haardt, "An introduction to the multi-user MIMO downlink," *IEEE Commun. Mag.*, vol. 42, no. 10, pp. 60–67, Oct. 2004.
- D. Gesbert, M. Kountouris, R. Heath, C.-B. Chae, and T. Salzer, "Shifting the MIMO paradigm," *IEEE Signal Process. Mag.*, vol. 24, no. 5, pp. 36–46, Sep. 2007.
- H. Zhang and H. Dai, "Cochannel interference mitigation and cooperative processing in downlink multicell multiuser MIMO networks," *EURASIP J. Wireless Commun. Netw.*, vol. 2004, no. 2, pp. 222–235, Dec. 2004.
- R. Zhang and L. Hanzo, "Cooperative downlink multicell preprocessing relying on reduced-rate back-haul data exchange," *IEEE Trans. Veh. Technol.*, vol. 60, no. 2, pp. 539–545, Feb. 2011.
- T. Marzetta, "Noncooperative cellular wireless with unlimited numbers of base station antennas," *IEEE Trans. Wireless Commun.*, vol. 9, no. 11, pp. 3590–3600, Nov. 2010.

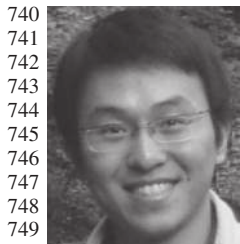
- [9] F. Rusek *et al.*, "Scaling up MIMO: Opportunities and challenges with very large arrays," *IEEE Signal Process. Mag.*, vol. 30, no. 1, pp. 40–60, Jan. 2013.
- [10] V. Cadambe and S. Jafar, "Interference alignment and degrees of freedom of the K-user interference channel," *IEEE Trans. Inf. Theory*, vol. 54, no. 8, pp. 3425–3441, Aug. 2008.
- [11] A. Molisch and M. Win, "MIMO systems with antenna selection," *IEEE Microw. Mag.*, vol. 5, no. 1, pp. 46–56, Mar. 2004.
- [12] A. Mohammadi and F. Ghannouchi, "Single RF front-end MIMO transceivers," *IEEE Commun. Mag.*, vol. 49, no. 12, pp. 104–109, Dec. 2011.
- [13] R. Mesleh, H. Haas, S. Sinanovic, C. W. Ahn, and S. Yun, "Spatial modulation," *IEEE Trans. Veh. Technol.*, vol. 57, no. 4, pp. 2228–2241, Jul. 2008.
- [14] M. Di Renzo, H. Haas, and P. M. Grant, "Spatial modulation for multiple-antenna wireless systems: A survey," *IEEE Commun. Mag.*, vol. 49, no. 12, pp. 182–191, Dec. 2011.
- [15] J. Wang, S. Jia, and J. Song, "Generalised spatial modulation system with multiple active transmit antennas and low complexity detection scheme," *IEEE Trans. Wireless Commun.*, vol. 11, no. 4, pp. 1605–1615, Apr. 2012.
- [16] L.-L. Yang, "Transmitter preprocessing aided spatial modulation for multiple-input multiple-output systems," in *Proc. IEEE 73rd VTC Spring*, 2011, pp. 1–5.
- [17] R. Zhang, L.-L. Yang, and L. Hanzo, "Generalised pre-coding aided spatial modulation," *IEEE Trans. Wireless Commun.*, vol. 12, no. 11, pp. 5434–5443, Nov. 2013.
- [18] A. Stavridis, S. Sinanovic, M. D. Renzo, and H. Haas, "Transmit precoding for receive spatial modulation using imperfect channel knowledge," in *Proc. IEEE 75th VTC Spring*, 2012, pp. 1–5.
- [19] C. Peel, B. Hochwald, and A. Swindlehurst, "A vector-perturbation technique for near-capacity multiuser communication—Part I: Channel inversion and regularization," *IEEE Trans. Commun.*, vol. 53, no. 1, pp. 195–202, Jan. 2005.
- [20] Q. Spencer, A. Swindlehurst, and M. Haardt, "Zero-forcing methods for downlink spatial multiplexing in multiuser MIMO channels," *IEEE Trans. Signal Process.*, vol. 52, no. 2, pp. 461–471, Feb. 2004.
- [21] M. Di Renzo and H. Haas, "Bit error probability of SM-MIMO over generalized fading channels," *IEEE Trans. Veh. Technol.*, vol. 61, no. 3, pp. 1124–1144, Mar. 2012.
- [22] J. A. Thomas and T. M. Cover, *Elements of Information Theory*, 2nd ed. Hoboken, NJ, USA: Wiley-Interscience, 2006.
- [23] R. Gallager, *Information Theory and Reliable Communication*. New York, NY, USA: Wiley, 1968.
- [24] M. S. John Proakis, *Digital Communications*, 5th ed. New York, NY, USA: McGraw-Hill, 2008.
- [25] M. Maleki, H. Bahrami, A. Alizadeh, and N. Tran, "On the performance of spatial modulation: Optimal constellation breakdown," *IEEE Trans. Commun.*, vol. 62, no. 1, pp. 144–157, Jan. 2014.
- [26] E. Telatar, "Capacity of multi-antenna Gaussian channels," *Eur. Trans. Telecommun.*, vol. 10, no. 6, pp. 585–595, Nov./Dec. 1999.
- [27] A. Edelman, "Eigenvalues and condition numbers of random matrices," Ph.D. dissertation, Dept. Math., MIT, Cambridge, MA, USA, 1989.
- [28] M. L. Eaton, *Multivariate Statistics: A Vector Space Approach*. Hoboken, NJ, USA: Wiley, 1983.



Lie-Liang Yang (M'98–SM'02) received the B.Eng. degree in communications engineering from Shanghai TieDao University, Shanghai, China, in 1988, and the M.Eng. and Ph.D. degrees in communications and electronics from Northern (Beijing) Jiaotong University, Beijing, China, in 1991 and 1997, respectively. From June 1997 to December 1997, he was a Visiting Scientist of the Institute of Radio Engineering and Electronics, Academy of Sciences of the Czech Republic. Since December 1997, he has been with the University of Southampton, U.K., where he is the Professor of wireless communications in the School of Electronics and Computer Science. His research has covered a wide range of topics in wireless communications, networking and signal processing. He has published over 290 research papers in journals and conference proceedings, authored/co-authored three books and also published several book chapters. The details about his publications can be found at <http://www-mobile.ecs.soton.ac.uk/lly/>. He is a Fellow of the IET, served as an associate editor to the IEEE TRANSACTIONS ON VEHICULAR TECHNOLOGY and *The Journal of Communications and Networks* (JCN), and is currently an associate editor to the *IEEE Access* and the *Security and Communication Networks (SCN) Journal*.



Lajos Hanzo received the B.S. degree in electronics in 1976 and the Ph.D. degree in 1983. In 2009, he was awarded the honorary doctorate "Doctor Honoris Causa" by the Technical University of Budapest. During his 38-year career in telecommunications he has held various research and academic posts in Hungary, Germany, and the U.K. Since 1986, he has been with the School of Electronics and Computer Science, University of Southampton, U.K., where he holds the Chair in telecommunications. He has successfully supervised 80+ PhD students, co-authored 20 John Wiley/IEEE Press books on mobile radio communications totalling in excess of 10 000 pages, published 1400+ research entries at IEEE Xplore, acted both as TPC and General Chair of IEEE conferences, presented keynote lectures, and has been awarded a number of distinctions. Currently, he is directing a 100-strong academic research team working on a range of research projects in the field of wireless multimedia communications sponsored by industry, the Engineering and Physical Sciences Research Council (EPSRC) U.K., the European Research Council's Advanced Fellow Grant, and the Royal Society's Wolfson Research Merit Award. He is an enthusiastic supporter of industrial and academic liaison and he offers a range of industrial courses. He is also a Governor of the IEEE VTS. During 2008–2012, he was the Editor-in-Chief of the IEEE Press and a Chaired Professor also at Tsinghua University, Beijing. His research is funded by the European Research Council's Senior Research Fellow Grant. He has over 20 000 citations. For further information on research in progress and associated publications please refer to <http://www-mobile.ecs.soton.ac.uk>



Rong Zhang (M'09) received the B.Sc. degree from Southeast University, China, in 2003 and the Ph.D. degree from Southampton University, U.K., in 2009. Before receiving the doctorate degree, he was an Engineer from August 2003 to July 2004 at China Telecom and a Research Assistant from January 2006 to May 2009 at Mobile Virtual Center of Excellence (MVCE), U.K. After being a post-doctoral Researcher from August 2009 to July 2012 at Southampton University, he took an industrial consulting leave from August 2012 to January 2013 for

Huawei Sweden R&D, as a System Algorithms Specialist. He was appointed as a Lecturer with the CSPC Group, ECS, Southampton University, in February 2013. He has over 30 journals in prestigious publication avenues such as IEEE and OSA and many more in major conference proceedings. He regularly serves as a Reviewer for IEEE transactions/journals and has several times served as a TPC member/Invited Session Chair of major conferences. He is the recipient of joint funding from MVCE and EPSRC and is also a Visiting Researcher under Worldwide University Network (WUN). More details can be found at <http://www.ecs.soton.ac.uk/people/rz>

AUTHOR QUERIES

AUTHOR PLEASE ANSWER ALL QUERIES

AQ1 = Please be informed that the capital letters were removed from the terms “multiple input multiple output,” “generalised pre-coded aided spatial modulation,” “symbol error ratio,” “bit error ratio,” “discrete-input continuous-output memoryless channel,” and “signal to noise ratio” in the Abstract per IEEE style and also in other occurrences of these terms in lines 88 to 91 and 305 for the sake of consistency. Please check if it is correct.

AQ2 = Please provide keywords.

AQ3 = Please check changes made in first footnote and the addition of an Acknowledgment Section.

AQ4 = Please check if “30 journals” should be “30 papers” instead.

END OF ALL QUERIES

IEEE
Proof